Manuscript prepared for Atmos. Chem. Phys.
with version 2015/09/17 7.94 Copernicus papers of the LaTeX class copernicus.cls.
Date: 15 June 2016

Seasonal variability of surface and column carbon monoxide over megacity Paris, high altitude Jungfraujoch and Southern Hemispheric Wollongong stations

Yao Té[1], Pascal Jeseck[1], Bruno Franco[2], Emmanuel Mahieu[2], Nicholas Jones[3], Clare Paton-Walsh[3], David W. T. Griffith[3], Rebecca R. Buchholz[4], Juliette Hadji-Lazaro[5], Daniel Hurtmans[6], and Christof Janssen[1]

[1]LERMA-IPSL, Sorbonne Universités, UPMC Univ Paris 06, CNRS, Observatoire de Paris, PSL Research University, F-75005, Paris, France
[2]Institut d'Astrophysique et de Géophysique, Université de Liège, B-4000 Liège, Belgique
[3]Center for Atmospheric Chemistry, Faculty of Science, Medicine & Health, University of Wollongong NSW 2522 Australia
[4]Atmospheric Chemistry Observations & Modelling Laboratory, National Center for Atmospheric Research, Boulder, CO, USA
[5]Sorbonne Universités, UPMC Univ. Paris 06, Univ. Versailles St-Quentin, CNRS/INSU, UMR 8190, LATMOS-IPSL, Paris, France
[6]Spectroscopie de l'Atmosphère, Service de Chimie Quantique et Photophysique, Université Libre de Bruxelles, Brussels, Belgium

Correspondence to: Yao Té (yao-veng.te@upmc.fr)

Abstract. ~~Carbon monoxide (CO) is an atmospheric key species due to its toxicity and its impact on the atmospheric oxidizing capacity, both factors affecting air quality.~~ The paper studies the seasonal variation of surface and column ~~altitude dependent seasonal variability of~~ CO at ~~the~~ three different sites (Paris, Jungfraujoch and Wollongong), with an emphasis on establishing a link between the CO vertical distribution and the nature of CO emission sources. We find the first evidence of a time-lag between surface and free tropospheric CO seasonal cycles in the Northern Hemisphere. The CO seasonal variability obtained from the total columns and from the free tropospheric partial columns shows a maximum around March-April and a minimum around September-October in the Northern Hemisphere (Paris and Jungfraujoch). In the Southern Hemisphere (Wollongong) this seasonal variability is shifted by about 6 months. Satellite observations by the IASI-MetOp and MOPITT instruments confirm this seasonality. Ground-based FTIR (Fourier Transform InfraRed) measurements ~~is demonstrated to~~ provide useful complementary information due to good sensitivity in the boundary layer. In situ surface measurements of CO volume mixing ratios in Paris and at Jungfraujoch reveal a time-lag of the near-surface ~~near surface~~ seasonal variability of about 2 months with respect to the total column variability at the same sites. The chemical transport model GEOS-Chem is employed to interpret our observations. GEOS-Chem sensitivity runs allow identification of ~~identifying~~ the emission sources influencing the seasonal cycle of CO. In Paris and at ~~on top of~~ Jungfraujoch,

the surface seasonality is mainly driven by anthropogenic emissions, while the total column seasonality is also controlled by air masses transported from distant sources. In ~~the case of~~ Wollongong, where the CO seasonality is mainly affected by biomass burning, no time shift is observed between surface measurements and total column data~~and above the boundary layer~~.

1 Introduction

~~Air is one of the most fundamental prerequisites for life and human beings inhale about 1500 litres of air per day. This air contains, besides of the major gaseous components nitrogen, oxygen and argon, reactive trace gases and small particles that are of concern for human health. The survey and control of these trace components, which affect air quality, have thus become a field of major importance for environmental research and public health authorities, especially in large cities. The quality of air is a function of time and space, which depends on many parameters such as geographic location, meteorological conditions, as well as sources and sinks of pollutants. It is thus strongly affected by natural and anthropogenic emissions.~~

Atmospheric carbon monoxide (CO) is an important trace gas. It has direct and indirect impact on air quality due to its toxicity and its effect on the atmospheric oxidizing capacity~~, due to its toxicity and its impact on the atmospheric oxidizing capacity and air quality . For example, have studied the seasonal phenomenon of poisoning mainly due to defect heating systems. have investigated the link between outdoor air pollution and cardiovascular hospital admissions. has studied the effect of pollution on the neurodevelopment~~. The major sources of CO are fuel and energy-related ~~energy related~~ industries, heating, motor vehicle transport, biomass burning, and the secondary oxidation of methane and of volatile organic compounds (VOCs such as isoprene and terpene), which are emitted by plants. Due to the fast reaction

$$\mathrm{CO} + \mathrm{OH} \rightarrow \mathrm{CO_2} + \mathrm{H}, \qquad \text{(R1)}$$

CO ~~(R1), carbon monoxide~~ is the major sink for the main atmospheric oxidation agent, the hydroxyl radical OH (Weinstock, 1969; Bakwin et al., 1994). A global increase of atmospheric CO thus leads to a decrease in global OH, which in turn augments the concentration of other, potentially harmful atmospheric trace gases (Logan et al., 1981; Thompson et al., 1990; Thompson, 1992) or potent greenhouse gases sensitive to oxidation such as methane, which contributes about one-third to the total sources of CO (Duncan et al., 2007; Holloway et al., 2000). Before 1980, there were only few measurements, which showed an increase of CO in the Northern Hemisphere (Khalil and Rasmussen, 1988; Zander et al., 1989), probably related to an increase of anthropogenic emissions (Novelli et al., 1998). From end of 1980 until 1997, CO has decreased (Khalil and Rasmussen, 1994; Novelli et al., 1994). Since then, few large episodic increases of CO, associated with unusual large forest fires, have been observed in the Northern Hemisphere (Novelli et al., 2003; Yurganov et al., 2004, 2005). Bekki et al. (1994) have observed a negative trend in CO, that was

attributed to the Mount Pinatubo eruption in June 1991. In the Southern Hemisphere no significant trends were observed (Brunke et al., 1990; Novelli et al., 2003). Global observations of CO were initiated through the start of the flask sampling program of the NOAA[1] Earth System Research Laboratory, Global Monitoring Division (Novelli et al., 1994, 1998, 2003). In parallel, CO total column observations were performed at several locations (Mahieu et al., 1997; Zhao et al., 1997; Rinsland et al., 1998, 1999, 2000).

This paper characterizes the CO seasonal variability at three ground-based FTIR sites: Paris megacity, high-altitude ~~remote~~ Jungfraujoch and Southern Hemisphere ~~Hemispheric~~ Wollongong. These sites have been selected for their representativeness of different environments (remote vs. moderate and high pollution sites, Northern vs. Southern Hemisphere) and meteorological conditions:

- Megacity of Paris (France): A high-resolution ~~high resolution~~ Fourier transform spectrometer from Bruker Optics (FTS-Paris) has been installed in 2006 on the campus of "Université Pierre et Marie Curie" in the centre of the French capital Paris (48°50'47"N, 2°21'21"E, 60 m asl). Since then, the instrument has been ~~is~~ continuously operated by LERMA~~.~~[2]. ~~The Île-de-France region covers a surface of about 12000 km^2 with more than 11 million inhabitants (16of the French population). The region has a relatively flat relief with an average elevation of 108m above sea level (asl) and is strongly influenced by the Atlantic Ocean. Between 1970 and 1990, levels of ambient were quite high and stable around 3.5ppmv . After 1990, a strong decrease was observed due to new European regulations for motorized vehicles (91/441/EEC Council Directive) becoming effective in the same year. Since 2008, the level in the Paris region has been quite stable with no significant trends.~~

- Jungfraujoch (Switzerland): The International Scientific Station of the Jungfraujoch (ISSJ) is located in the Swiss Alps (46°33'N, 7°58'48"E, 3580 m asl). Two FTIR instruments have been used at that site, a homemade FTIR from 1984 to 2008 and a commercial Bruker IFS 120 HR from the early 1990 to present~~, providing one of the longest observational time series for a variety of atmospheric gases~~. University of Liège (Belgium) is responsible for the operation of the infrared instruments at Jungfraujoch. ~~Due to its elevation, the site primarily probes the European free troposphere and layers above.~~

- Wollongong (Australia): The station is located in the Southern Hemisphere at Wollongong University (34°24'22"S, 150°52'44"E, 30 m asl). The instrument, which is also a commercial high-resolution Fourier transform spectrometer (Bruker IFS 125HR), is operated by the University of Wollongong and provides data since 1996.

[1] National Oceanic and Atmospheric Administration
[2] Laboratoire d'études du Rayonnement et de la Matière en Astrophysique et Atmosphères

All three ground-based FTIR ~~(Fourier Transform Infrared)~~ spectrometers are part of NDACC (Network for the Detection of Atmospheric Composition Change) and/or TCCON (Total Carbon Column Observing Network) networks and have monitored ~~monitor~~ the concentration of CO for several years. Paris is the first ground-based FTIR station located in a European megacity which provides rare hot spot measurements of atmospheric species related to anthropogenic activities. The remote high-altitude Jungfraujoch station provides one of the longest observational time series for a variety of atmospheric gases. Wollongong is a station exposed to moderate levels of pollution and is located at the East coast of Australia and about 80 km from the South of Sydney. Here, we present NDACC analysis data on the seasonal variations of CO and compare the results from the different sites. The ground-based ~~These~~ remote sensing measurements are compared with results from the satellite instruments IASI-MetOp (Infrared Atmospheric Sounding Interferometer (Tournier et al., 2002)) and MOPITT (Measurements Of Pollution In The Troposphere (Drummond and Mand, 1996)). With respect to satellite measurements, ground-based FTIR instruments are more sensitive to the boundary layer and can therefore provide complementary data which we compare with in situ measurements at the surface. Due to specific conditions at the ground, the surface and the total column seasonalities might differ from each other. Using ~~surface insitu measurements. Using custom~~ GEOS-Chem modeling ~~model~~ (Goddard Earth Observing System - chemical transport model (CTM), Bey et al. (2001)) simulations, we investigate the impact of local sources on the lower partial column and its variability as compared to the total column.

The paper is structured as follows. In section 2, the remote sensing instruments and measurements are ~~??, the different ground-based and satellite instruments will be~~ described. Section 3 presents the in situ analyser measurements and the GEOS-Chem model simulation data. Section 4 shows the CO total column variability obtained from the remote sensing data and the one from the surface in situ measurements. Both results are compared to the GEOS-Chem model simulations, which is also used to identify emission sources at each site~~Section presents the measurement data, which are then discussed and compared insection 4~~ .

2 Remote sensing instruments and measurements~~Instrument description~~

2.1 Instrumentation and measurements at Paris, France

The ~~The Fourier transform spectrometer (~~FTS-Paris is a ~~) is a model IFS 125 HR~~ Michelson interferometer from Bruker Optics. Table 1 lists technical details on the ~~, cf. . Its maximum optical path difference is up to 258cm, which corresponds to a spectral resolution of 2.4×10^{-3}cm^{-1}.The instrument is equipped with IR optical elements (entrance window and beamsplitter, detector), suited for~~ ground-based FTIR instruments as well as the configuration used for the measurements~~atmospheric observations~~ . Solar absorption spectra are acquired ~~measurements are achieved~~ by coupling the FTS ~~FTS-Paris instrument~~ to a sun-tracker ~~(model A547 from Bruker Optics)~~ installed on the roof ter-

race. The solar disk is tracked with an accuracy of less than 1 arcmin. Using ~~The spectra contain rovibrational signatures of many atmospheric constituents, including numerous atmospheric pollutants. The spectral range determined by the above choice of optical elements and detectors is limited to the range between 1 and 5.4μm. It is further narrowed down using~~ appropriate band pass filters allows the optimisation of the signal-to-noise ~~in order to optimise the signal to noise~~ ratio when focussing on specific target gases. The Paris instrument is part of TCCON (TCCON-Paris station). But for the present CO study, the FTS-Paris uses optical elements corresponding ~~For CO , the chosen optical filter and the InSb detector allow to cover the spectral domain from 3.8 to 5.1μm, which corresponds~~ to a typical NDACC configuration. More instrumental details and different measurement configurations are given ~~specified~~ elsewhere (Té et al., 2010, 2012).

~~Continuous in situ measurements of the surface concentration are performed using a commercial CO11M analyser (Environnement SA). The operating principle of the analyser is based on the infrared absorption at 4.67μm, which is the same spectral band covered by the FTS-Paris. Ambient atmospheric air is drawn from the building rooftop into the analyser via PTFE tubing using a diaphragm pump, which is limited to a gas flow of 80 litres per hour. The pumped air is analysed in a 20cm length multi-path absorption cell with an absorption path length of 5.6m, using a globar IR source and a photoconductive detector. The CO11M analyser has a sensitive range between 0.1 and 200ppmv, with an uncertainty of 50ppbv for each individual measurement. Recorded values are time averages over 15 minutes.~~

2.2 ~~Instrumentation at Jungfraujoch, Switzerland~~

~~The Jungfraujoch station in Switzerland is currently equipped with a Bruker IFS 120 HR, which is part of the NDACC network. A thorough description of the instrumentation is given in . Infrared solar spectra are recorded under clear-sky conditions and, thanks to the high altitude, the interference by water vapour is significantly limited in these observations. The instrumental setup is similar to the one used in Paris, although spanning here the 4.4 to 6μm range. The spectra are recorded with an optical path difference alternating between 114 and 175cm. The integration time is either 135, 404 or 1035s, corresponding to 3 or 9 scans of 45 s, or 15 scans of 69s. High resolution observations are only recorded under slowly varying geometry, i.e. for zenith angles lower than $\sim 70^{o}$.~~

2.2 ~~Instrumentation at Wollongong, Australia~~

~~The Wollongong instrument is also an IFS 125 HR Michelson interferometer from Bruker Optics. Using the NDACC mode, total and partial column data are produced using 3 micro-windows from the 4.6μm band . The instrument setup is also similar to the Paris and Jungfraujoch spectrometers, with an optical path difference of 257cm, with two spectra co-added for an integration time of 206 seconds.~~

Measurements of surface at Wollongong are combined from two high-precision in situ FTIR trace gas analysers . The analysers use an IR source, modulated through a Michelson interferometer with a beamsplitter. The modulated IR beam is passed through a dried atmospheric sample within a White cell in a 24 metre folded-path and subsequently detected by thermoelectrically cooled MCT (Mercury Cadmium Telluride) detector. Ambient air is measured daily over 23.5 hours, with 30 minutes reserved for calibration using constant composition air. Ambient air is flushed through an inlet line at 5L/min and sample air is continuously drawn from this line through the instrument at 1L/min. The SpectronusTM software (Ecotech P/L, Knoxfield, VIC, Australia) is used to automate internal valve control and stabilise parameters, such as flow, pressure and temperature. Recorded spectra are averaged over 3 minutes. Non-linear least-squares fitting of occurs in two broad spectral regions (from 4.33 to 4.65μm and from 4.46 to 4.76μm), using the program MALT (Multiple Atmospheric Layer Transmission,). Data are reported as dry-air mole fraction, with a total relative measurement uncertainty below 1. Wollongong measurements were first analysed by and are publicly available as 10 minute averages via PANGAEA (doi:10.1594/PANGAEA.848263).

2.2 Satellite instruments

The IASI Michelson interferometer (Infrared Atmospheric Sounding Interferometer, is flying on-board the Meteorological operation (MetOp) polar orbit platform. The first platform (MetOp-A) was launched on October 19, 2006 and data have been provided operationally since October 2007. It operates at an altitude of around 817km on a sun-synchronous orbit with a 98.7^{o} inclination to the equator. It overpasses each region twice a day. The MetOp platform has a swath of 30 views of 50km by 50km comprising four off-axis pixels of 12km diameter footprint each at nadir. A second platform (MetOp-B) was launched in September 2012 and the launch of the third and last platform (MetOp-C) is scheduled in October 2018. IASI observations provide an important contribution to the monitoring of atmospheric composition over time .

The MOPITT instrument is on-board the NASA's Terra spacecraft in a sun-synchronous polar orbit at an altitude of 705km. The satellite was launched on December 18, 1999. MOPITT has been operational since March 2000. The instrument uses the technique of gas-filter correlation radiometry based on the IR absorption bands of to retrieve the vertical profiles of CO. The horizontal footprint of each MOPITT retrieval is 22 km by 22 km.

In order to be compared to the ground-based FTIR data, satellite data were selected when they are located in a 30 km $\times$ 30 km square centered at the site location: 0.15^{o} around the site latitude and 0.23^{o} around the site longitude.

3 Data Analysis

2.1 Column data from Paris

~~Solar spectra were recorded within 3min at the maximum spectral resolution of 0.0024cm^{-1}.~~ Only clear sky spectra were analysed~~admitted to analysis~~. Available solar spectra cover the time period from May 2009 to the end of 2013, with only very few spectra (about 400 spectra during 19 measurement days) for the period between 2009 and 2010. Between 2011 and 2013, spectra acquisition was more frequent ~~became more regular~~ and more than 4500 spectra from 117 measurement days were recorded and analysed. The absorption lines of each atmospheric species observed in the solar spectra are used to retrieve its abundance in the atmosphere by appropriate radiative transfer and inversion algorithms (Pougatchev and Rinsland, 1995; Zhao et al., 1997; Hase et al., 2006). We have used the PROFFIT algorithm developed by F. Hase to analyse the Paris data using the HITRAN 2008 spectral database (Rothman et al., 2009)~~as spectral database~~. PROFFIT is a code especially adapted for the analysis of solar absorption spectra from the ground and it has been widely applied and tested (Hase et al., 2004; Duchatelet et al., 2010; Schneider et al., 2010; Té et al., 2012; Viatte et al., 2011). For the retrieval of CO~~CO~~, we have selected two micro-windows. The $2110.4 - 2110.5\,\mathrm{cm^{-1}}$ micro-window is centred around the weak $R(3)$ line of ^{13}CO~~R(3) line~~, which is more sensitive to CO at higher altitudes and the $2111.1 - 2112.1\,\mathrm{cm^{-1}}$ micro-window around the strongly saturated $P(8)$ line of ^{12}CO~~P(8) line~~. The left and right wings of that line are particularly sensitive to CO in the Planetary Boundary Layer (PBL). The retrieval uses a grid with 49 altitude levels ~~. This corresponds to a much thinner atmospheric layering than the effective vertical resolution indicated by the averaging kernels (Rodgers, 1990). Figure 1. shows that the retrieval of essentially provides two independent measurement points of in the troposphere: the first point delivers maximal information in the altitude range between 0~~ and, on average, there are about 2.7 degrees of freedom (DOF)~~1000m andthus well represents the PBL. The second one is representative of the upper troposphere, with a maximum around 8-9km~~. The uncertainties in the CO column density and the profile stem from a variety of sources. These sources have been investigated in detail by Té et al. (2012), following the procedure outlined by Rinsland et al. (2000). According to this evaluation, the random uncertainty is around 2.5%. Concerning the systematic uncertaintianties of about 3 to 6.8% (Té et al., 2012), the largest source is linked to the quality of available spectroscopic parameters (line intensity and air-broadened half-width uncertainties in Rothman et al. (2009)), which is similar for the three sites.

2.1 Instrumentation and measurements at Jungfraujoch, Switzerland

The Jungfraujoch station in Switzerland is part of NDACC and the instrumental setup is similar to the one in Paris, cf. Table 1. A thorough description of the instrumentation is given by Zander et al. (2008). Infrared solar spectra are recorded under clear-sky conditions and, thanks to the high altitude, the interference by water vapour is very low. The integration time is either 135, 404 or 1035 s, corresponding to 3 or 9 scans of 45 s, or 15 scans of 69 s. High resolution observations are only recorded under slowly varying geometry, i.e. for zenith angles lower than $\sim 70^{\circ}$.

2.2 ~~Column data from Jungfraujoch~~

The Jungfraujoch data set corresponds to an update of the CO time series described by Dils et al. (2011)~~in~~. It covers ~~here~~ the January 2009 to December 2013 time period and includes 1733 individual spectra recorded on 539 different days. Mean signal-to-noise ratio (S/N) is 2930, with the 2nd percentile still being ~~2nd percentile still~~ above 1000. The ~~We used the~~ SFIT-2 (v3.91) algorithm (Rinsland et al., 1998) ~~which is~~ based on the semi-empirical implementation of the Optimal Estimation Method (OEM) of Rodgers (1990) is used, allowing retrieval of information on the vertical profile of most FTIR target gases. The standard NDACC approach for the CO retrieval is adopted, to simultaneously fitting ~~fitting simultaneously~~ three micro-windows spanning the 2057.7 – 2058.0, 2069.56 – 2069.76 and 2157.3 – 2159.15 ~~2057.7 – 2058.0, 2069.56 – 2069.76 and 2157.3 – 2159.15~~ cm^{-1} intervals. The line parameters correspond to the standard release of HITRAN 2004 (Rothman et al., 2005), including the August 2006 updates (e.g. Esposito et al., 2007). The a priori mixing ratio profiles for all interfering molecules (main telluric absorptions by N_2O, O_3, H_2O and CO_2) correspond to a mean of the 1975-2020 version 4 ~~simulation performed for the Jungfraujoch by the~~ WACCM model (the Whole Atmosphere Community Climate Model; https://www2.cesm.ucar.edu/working-groups/wawg) simulation performed for the Jungfraujoch. The CO a priori vertical distribution combines WACCM results above 15.5 km, ACE-FTS occultation measurements between 6.5 and 15.5 km (version 2.2, Clerbaux et al., 2008) and extrapolation ~~extrapolation~~ of ACE-FTS data down to the station altitude, ending at 137 ppbv in the first retrieval layer (3.58 – 4.23~~3.58 – 4.23~~ km). Additional retrieval settings include a S/N ratio of 150 for inversion, the a priori covariance matrix, with diagonal elements close to 30%/km in the troposphere and extra-diagonal elements computed assuming a Gaussian inter-layer correlation half-width length of 4 km. Objective evaluation of the resulting typical information content indicates that 2 independent pieces of information are available (DOF ~~DOFS~~ of 2.2 on average). ~~The second eigenvector provides some vertical resolution and the determination of partial columns below and above 7.18km is only marginally impacted by the a priori .~~ Typical random uncertainties have been evaluated at 2 – 3~~2-3~~% for the total columns and 5% for the 3.58 – 7.18 km partial columns.

2.2 Instrumentation and measurements at Wollongong, Australia

The Wollongong instrument is part of both NDACC and TCCON. The instrument setup is similar to the Paris and Jungfraujoch spectrometers (see Table 1). Using the NDACC configuration, CO total and partial column data are produced using 3 micro-windows in the 4.6 μm band of CO (Zeng et al., 2015).

2.3 ~~Column data from Wollongong~~

The analysis of the Wollongong NDACC data is very similar to ~~follows very closely~~ the method described in section 2.2 ~~above in section 3.2~~ for the Jungfraujoch data. The algorithm used was SFIT4 v9.4.4 (https://wiki.ucar.edu/display/sfit4/Infrared+Working+Group+Retrieval+Code,+SFIT), an updated version of SFIT2 used in the Jungfraujoch analysis. SFIT4 has inherited the same forward model and inverse method but with a number of enhancements (not required in the CO analysis), and ~~for the retrieval~~ gives the same results in the CO retrieval~~result~~. For the Wollongong data, HITRAN 2008 was adopted (Rothman et al, 2009), the mean of the 1980-2020 WACCM version 4 run used as the a priori CO profile (and a 4 km Gaussian interlayer correlation), with the a priori covariance matrix set to 1 standard deviation of the WACCM profiles. A measurement signal-to-noise ~~signal to noise~~ ratio of 200 was assumed. This gives a mean DOF ~~gave a mean DOFS~~ of 2.7. The version 4 WACCM profiles were also used for the a priori profiles of all actively fitted interfering ~~inferring~~ gases (O_3, H_2O, N_2O, CO_2, etc.). The error analysis used a NDACC community Python tool to estimate errors assuming a solar zenith angle of 50.2°, representing the mean zenith angle for all Wollongong spectra. The resulting CO total column random errors were calculated to be 2.2%.

2.3 Satellite ~~Data from the satellite~~ instruments and measurements

The IASI Michelson interferometer (Infrared Atmospheric Sounding Interferometer, Tournier et al. (2002); Blumstein et al. (2004)) is flying on-board the Meteorological operation (MetOp) polar Orbit platform. The first platform (MetOp-A) was launched on October 19, 2006 and operational data have been provided since October 2007. IASI operates at an altitude of around 817 km on a sun-synchronous orbit with a 98.7° inclination to the equator. It overpasses each region twice a day. The MetOp platform has a swath of 30 views of 50 km by 50 km comprising four off-axis pixels of 12 km diameter footprint each at nadir. A second platform (MetOp-B) was launched in September 2012 and the launch of the third and last platform (MetOp-C) is scheduled for October 2018. IASI observations provide an important contribution to the monitoring of atmospheric composition over time (Clerbaux et al., 2009).

The IASI-MetOp is a Fourier transform spectrometer with a medium spectral resolution of 0.5 cm^{-1} and a radiometric noise of about 0.2 K at 280 K using nadir viewing and working in the thermal infrared (TIR) range extending from 645 to 2760 cm^{-1} with no gaps. The CO products (L2) ~~from the IASI sounder on the MetOp satellite~~ are downloaded from the ETHER database, cf. http://www.pole-ether.fr, for the period from January 1, ~~1 January~~ 2009 to December 31, ~~31 December~~ 2013. The total column data were generated from the IASI radiance spectra in the 4.7 μm spectral range and from IASI L2 meteorological data (surface and vertical profile of temperature, humidity vertical profile and cloud cover) (August et al., 2012), using the Fast Optimal Retrievals on Layers for IASI (FORLI) code (Hurtmans et al., 2006). The CO total columns were compared to other CO

satellite data (George et al., 2009), from which a DOF value of about 2 was provided and a relative uncertainty between 4% and 10% could be estimated. The total columns are calculated from the ground altitude to 60 km height. For this paper, we also provide ~~have also~~ additional vertical volume mixing ratio (VMR) profiles ~~profile~~ and partial columns in the PBL and in the troposphere layers around Île-de-France; as well as the partial columns above 4 km height around the Jungfraujoch site.

The MOPITT instrument (Drummond and Mand, 1996; Deeter et al., 2004) is on-board the NASA's Terra spacecraft in a sun-synchronous polar orbit at an altitude of 705 km. The satellite was launched on December 18, 1999. MOPITT has been operational since March 2000. The instrument uses the technique of gas-filter correlation radiometry based on the IR absorption bands of CO to retrieve the vertical profiles of CO. The horizontal footprint of each MOPITT retrieval is 22 km by 22 km.

The MOPITT data were downloaded from the NASA website, cf. https://eosweb.larc.nasa.gov/datapool. We are using ~~the available data of the~~ version 6 retrievals of CO vertical profiles and total columns, for the period from the beginning of 2009 to the end of 2013. The MOPITT retrieval history can be found at the link https://www2.acd.ucar.edu/mopitt/products. Since version 5 of the MOPITT retrieval algorithm, TIR (4.7 μm) radiances are combined with the near IR (2.3 μm) daily radiances to improve the sensitivity to lower tropospheric CO over land. The DOF value is about 2 (Worden et al., 2010). The retrieved vertical VMR profile is reported on 10 pressure levels (at the surface and every hundred hPa between 900 and 100 hPa). The retrieved CO total columns are obtained by integrating the retrieved VMR profile. In this paper, we are using the level 2 TIR/NIR products.

In order to be compared to the ground-based FTIR data, satellite data were selected when they are located in a 30 km $\times$ 30 km square centered at the site location: 0.15° around the site latitude and 0.23° around the site longitude.

3 In situ analyser measurements and GEOS-Chem model simulation data

3.1 Surface in situ measurements at Paris

Continuous in situ measurements of the CO surface concentration are performed using a commercial analyser (CO11M , Environnement SA). The operating principle of the CO analyser is based on the CO infrared absorption at 4.67 μm, which is the same spectral band covered by the FTS-Paris. Ambient atmospheric air is drawn from the building rooftop into the analyser via PTFE tubing using a diaphragm pump, which is limited to a gas flow of 80 litres per hour. The pumped air is analysed in a 20 cm length multi-path absorption cell with an absorption path length of 5.6 m, using a globar IR source and a photoconductive PbSe detector. The CO analyser has a sensitive range between 0.1 and 200 ppmv, with an uncertainty of 50 ppbv for each individual measurement. Recorded values are time averages over 15 minutes. For the present paper, daily in situ surface CO measurements are available for the whole period between beginning of 2009 and end of 2013.

3.2 Surface in situ measurements in Switzerland

Swiss in situ surface data are from the Swiss National Air Pollution Monitoring Network (NABEL), which is a network of 16 observation sites distributed throughout Switzerland in order to measure and record long-term measurement series of air pollutants. The NABEL monitoring network is operated by EMPA. The monitoring stations are representative of different pollution levels. The monthly averaged data were obtained from the annual reports published by the Swiss OFEV (Office fédéral de l'Environnement, http://www.bafu.admin.ch/publikationen/00016). For the paper, we have focussed on the urban sites Bern, Lausanne, Lugano and Zürich as well as the remote mountain station of Jungfraujoch.

3.3 Surface in situ measurements at Wollongong

Results of surface CO at Wollongong were obtained from two high-precision in situ FTIR trace gas analysers (Griffith et al., 2012). The analysers use an IR source, modulated through a Michelson interferometer with a CaF_2 beamsplitter. The modulated IR beam is passed through a dried atmospheric sample within a White cell in a 24 m folded-path and subsequently detected by thermoelectrically cooled MCT (Mercury Cadmium Telluride) detector. Ambient air is measured daily over 23.5 hours, with 30 minutes reserved for calibration using constant composition air. Ambient air is flushed through an inlet line at 5 L/min and sample air is continuously drawn from this line through the instrument at 1 L/min. The SpectronusTM software (Ecotech P/L, Knoxfield, VIC, Australia) is used to automate internal valve control and stabilise parameters, such as flow, pressure and temperature. Recorded spectra are averaged over 3 minutes. Non-linear least-squares fitting of CO occurs in two broad spectral regions (from 4.33 to 4.65 μm and from 4.46 to 4.76 μm), using the program MALT (Multiple Atmospheric Layer Transmission, Griffith (1996)). Data are reported as dry-air mole fraction, with a total relative measurement uncertainty below 1%. Wollongong CO measurements were first analysed by Buchholz et al. (2016) and are publicly available as 10 minute averages via PANGAEA (doi:10.1594/PANGAEA.848263). In situ data was monthly averaged and selected to cover the period from June 2012 to May 2013.

3.4 Data from the GEOS-Chem model

The global 3-D chemical transport model GEOS-Chem (version 9-02: http://acmg.seas.harvard.edu/geos/doc/archive/man.v9-02) can be used to simulate ~~allows for simulating~~ global trace gas (more than 100 tracers) and aerosol distributions. The model is driven by the Goddard Earth Observing System v5 (GEOS-5) assimilated meteorological fields from the NASA Global Modeling Assimilation Office (GMAO), which are at a native horizontal resolution of $0.5^o \times 0.667^o$. The GEOS-5 data describe the atmosphere from the surface up to 0.01 hPa with 72 hybrid pressure-σ levels, at a 6 h temporal frequency (3 h for surface properties and mixing depths). In this study, we use the

degraded GEOS-5 meteorological fields as model input to a $2^o \times 2.5^o$ horizontal resolution and 47 vertical levels, lumping together levels above ~ 80 hPa. We apply here the standard full chemistry GEOS-Chem simulation, including detailed O_3 – NO_x – Volatile Organic Compound (VOC) – aerosol coupled chemistry (Bey et al. (2001); Park et al. (2004); with updates by Mao et al. (2010)).

Tropospheric CO is emitted from anthropogenic, biomass burning and biofuel burning sources, as well as from the degradation of many VOCs. The emission inventory of the emissions database for Global Atmospheric Research (EDGAR; http://edgar.jrc.ec.europa.eu) v3.2 (Olivier and Berdowski, 2001) is the global reference for anthropogenic emissions of CO, NO_x, SO_x, and NH_3. For global anthropogenic sources of Non-Methane VOCs (NMVOCs), GEOS-Chem uses the REanalysis of the TROpospheric chemical composition (RETRO; http://gcmd.gsfc.nasa.gov/records/GCMD_GEIA_RETRO) emission inventory (Schultz et al., 2007) for the base year 2000. However, these global inventories may be overwritten by regional emission inventories such as over Europe, where the anthropogenic emissions of CO, NO_x, SO_x, NH_3, propene, acetaldehyde, methyl ethyl ketone and higher C3 alkanes are provided by the European Monitoring and Evaluation Programme (EMEP; http://www.ceip.at) regional inventory for the year 2010 (Benedictow et al., 2010). All these global and regional inventories are scaled to the years of interest according to the method described by van Donkelaar et al. (2008). Anthropogenic sources of ethane and propane are derived from an offline simulation (Xiao et al., 2008). The global biomass burning emissions are provided by the Global Fire Emissions Database (GFED) v3 (van der Werf et al., 2010) and the global biogenic emissions are obtained with the Model of Emissions of Gases and Aerosols from Nature (MEGAN) v2.1 (Guenther et al., 2006)). Methane concentrations in GEOS-Chem are based on measurements from the NOAA Global Monitoring Division flask measurements.

The GEOS-Chem data set employed in the present work covers the period from January 2009 to May 2013 and is derived from a July 2005 to May 2013 simulation, for which the GEOS-5 meteorological fields are available. A 1-year run preceding this simulation was used for chemical initialization of the model. The model outputs consist of CO VMR profiles simulated at the closest pixel to each station and saved at a 3 h time step. The vertical resolution and the sensitivity of the FTIR retrievals have been taken into account for the comparisons involving GEOS-Chem results: the individual VMR profiles produced by the model have been first regridded onto the vertical layer-scheme adopted at each station, then daily averaged and finally smoothed by convolution with the FTIR averaging kernels (AVKs) according to the formalism of Rodgers and Connor (2003). The regridding method used here is a mass conservative interpolation that preserves the CO total mass simulated above the altitude of the station (the CO mass below is ignored). The AVKs employed for smoothing are seasonal averages (over March – May, June – August, September – November and December – February, respectively) derived from the individual retrievals of the 2009 – 2013 FTIR data sets. The smoothing did not change the comparison results between the model and our observations (difference smaller than 1%)

3.5 ~~Data from in situ surface analysers~~

~~At Paris, daily in situ surface measurements are available for the whole period between beginning of 2009 and end of 2013. At Wollongong, we calculate monthly averages of the in situ data, covering the period from June 2012 to May 2013. Swiss in situ surface data are from the Swiss National Air Pollution Monitoring Network (NABEL), which is a network of 16 observation sites distributed throughout Switzerland in order to measure and record long-term measurement series of air pollutants. The NABEL monitoring network is operated by EMPA (Air Pollution / Environmental Technology Department). The monitoring stations are representative of different pollution levels. The monthly averaged data were obtained from the annual reports published by the Swiss OFEV (Office fdral de l'Environnement,). For the paper, we have focussed on the urban sites (Bern, Lausanne, Lugano and Zürich)and the remote mountain site of Jungfraujoch~~.

4 Seasonal variability

4.1 Remote sensing observations

Figure 1 ~~2~~ shows the CO total columns of the three ground-based FTIR sites from 2009 to the end of 2013. The data from Paris are less numerous than from ~~as compared to~~ the other two sites, because measurements are not ~~yet~~ fully automated and spectral acquisitions are only launched when clear sky is expected for more than half of the daytime. Moreover, from 2009 to 2010, Paris CO spectra were recorded only during intensive measurement campaigns, and not on a regular ~~regularly~~ basis. As expected, the CO abundance is higher in the Northern Hemisphere. The CO column mean value is about 2.1×10^{18} molecules/cm^2 at Paris which is almost twice as high as the value at Wollongong (1.3×10^{18} molecules/cm^2). The CO mean value of 1.1×10^{18} molecules/cm^2 at Jungfraujoch is quite low due to the site's height. ~~elevation; the low altitude layers with the highest concentrations of that contribute at the other sites cannot do so here.~~

All three sites clearly display a ~~panels show clearly the~~ seasonal variability of CO. For its characterisation, we ~~We~~ have used a sine function (Eq. (1)). This is in agreement with previous studies conducted by Rinsland et al. (2000, 2001, 2007) and Zhao et al. (2002), but in comparison to Rinsland et al., we have removed the linear term, because our data sets do not show any significant trend: ~~to characterize this seasonal variability.~~

$$y = y_0 + A \sin\left(\pi \frac{t - t_c}{w}\right). \quad (1)$$

Here y represents the abundance of CO (in total or partial columns or volume mixing ratio); y_0 is the mean value (offset); A and w respectively are ~~are respectively~~ the amplitude and the half-period of the seasonal cycle~~(assumed to be sinusoidal)~~; t and t_c the date and the phase shift~~in days~~. Table 2 summarizes the fit results for ~~fitted~~ w and A obtained at the three sites.

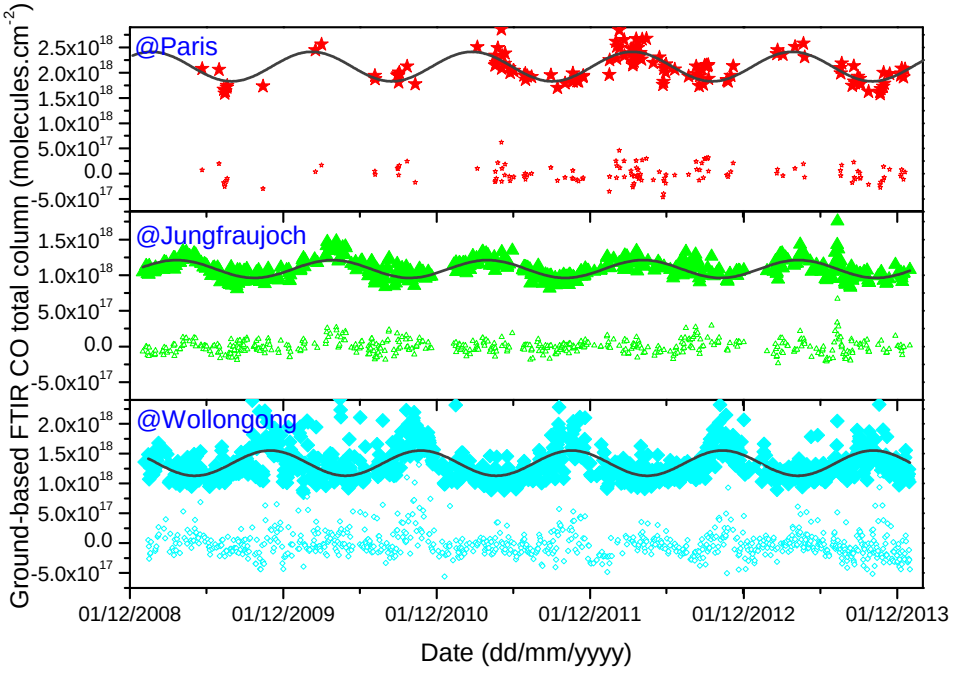

Figure 1. CO total columns retrieved by ground-based FTIR instruments at Paris (top), Jungfraujoch (middle) and Wollongong (bottom). Dark gray lines present CO seasonal variability at each station fitted with sine functions. Open symbols represent the residuals from the sine fit.

For the Northern Hemisphere (Paris and Jungfraujoch), the maximum is observed around March-April and the minimum around September-October. The average amplitude of the seasonal variability is about (13 ± 3)~~(14 ± 2)~~% of the column average and the ~~. The~~ average half-cycle is about 188 ± 4 days for both Northern hemispheric sites~~184 ± 4 days~~. For Paris, the value $w = 191 \pm 3$ days ~~($w = 191$days)~~ is slightly, but not significantly higher, probably due to the lack of data before 2011. This seasonal variability is also observed by Rinsland et al. (2007) at Kitt Peak, which is the US National Solar Observatory at 2.09 km altitude located in the Northern Hemisphere, by Barret et al. (2003) at the Jungfraujoch, and by Zhao et al. (2002) for Northern Japan. Our observations also agree with a recent 11 years climatology on purely tropospheric CO columns at Northern hemispheric sites (Zbinden et al., 2013), where observed maxima fall within the period from February to April. In the Southern Hemisphere, we observe an expected shift of 6 months as compared to the Northern Hemisphere, with a maximum in October and a minimum in April. The average half-period is about 178 ± 1 days. We also note that the relative amplitude of the seasonal variation is slightly higher at Wollongong (17~~16as compared to 14~~%) than at Paris, but it remains close ~~at Paris), but still~~

within error bars. Interestingly, the relative amplitude is lowest at Jungfraujoch, where the impact of the local surface emissions is small.

The seasonal variability of CO is also observed by the satellite IASI-MetOp and MOPITT instruments, cf. Fig. 2 3 and Table 2. One of the advantages of the satellite measurements is their spatial coverage. In general, the period and the amplitude of the seasonal variability obtained from the satellite data agree with the corresponding values from the ground-based FTIR measurements. For the Jungfraujoch station high altitude site Jungfraujoch , the satellite data need to be recalculated

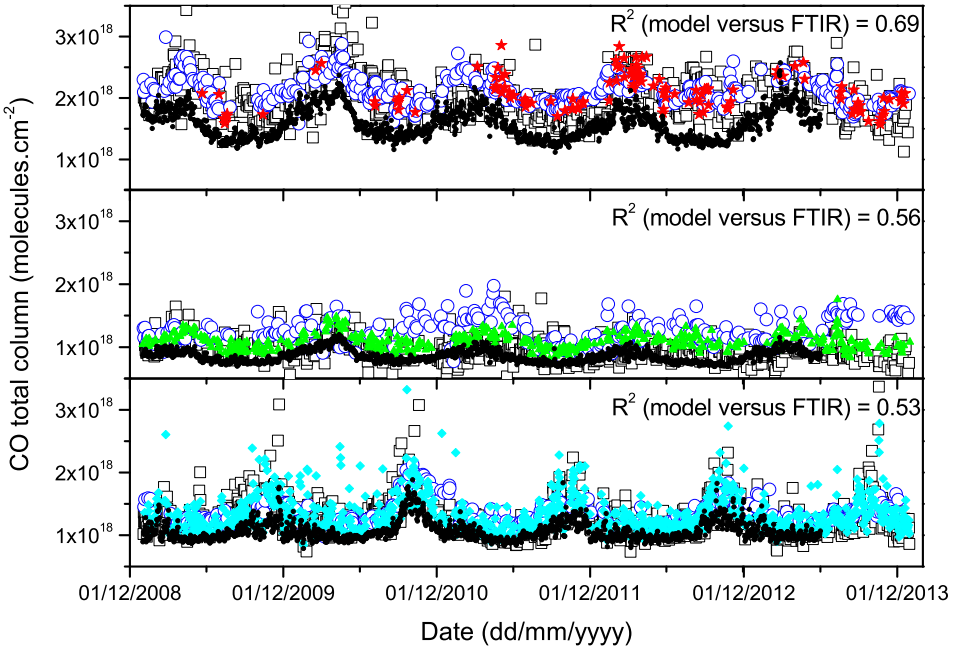

Figure 2. Time series of CO columns from satellite instruments and ground-based ground based FTIR are given for Paris, Jungfraujoch and Wollongong (. Total columns from top to bottom). IASI-MetOp and MOPITT columns are displayed as (black open squares) and MOPITT (blue open circles) for Paris (top panel) and Wollongong (bottom panel); partial columns for Jungfraujoch (middle panel). Ground-based FTIR CO total columns are shown by (red stars, green triangles and cyan diamonds for Paris, Jungfraujoch and Wollongong, respectively). GEOS-Chem CO total columns are indicated by shown as black small full circles in black colour.

in order to correspond to the column between the ground site altitude and the top of the atmosphere (Barret et al., 2003), because the large satellite footprint not only includes does not only include the site, but also neighboring areas of lower altitude. Concerning the IASI-MetOp data, the contributions from levels below the Jungfraujoch altitude have been subtracted from the total columns. For the MOPITT data, we extracted the retrieved CO profile for Jungfraujoch and interpolated the lower pressure levels in a thinner vertical grid in order to calculate the column between the given

ground altitude and the top of the atmospherebetween the ten pressure levels for a better vertical resolution. MOPITT measurements are performed for specific ground altitudes which, however, are not made available. We have assumed a ground altitude of about 1100 m which is the mean altitude for the Bern canton,[3] to which the Jungfraujoch site belongs. Partial columns above 1100 m were then calculated using the interpolated CO vertical profiles and daily NCEP meteorological pressure and temperature profiles. Both interpolated satellite partial columns of are plotted in Fig. 3 for Jungfraujoch. Data from the ground-based FTIR instruments and the satellites are in good agreement. This is demonstrated in Fig. 34, where the satellite data are plotted against the ground-based measurements. The good agreement is indicated by robust fits yielding slopes of 0.98 for Paris, 0.91 for Jungfraujoch and 0.99 for Wollongong. The robust fit regression is based on a process called called iteratively reweighted least squares (Street et al., 1988) and . The robust fitting method is less sensitive than ordinary least squares to large changes in small parts of the data.

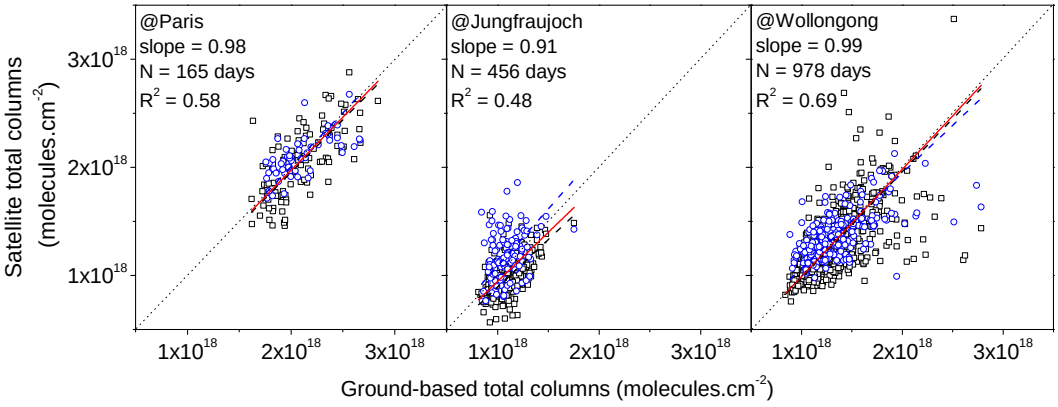

Figure 3. Correlation between satellites (IASI and MOPITT) and ground-based FTIR total columns at the three different sites, IASI data are in black squares and MOPITT data in blue circles. The dark dotted line and the blue one are the robust regression fit results for respectively IASI-MetOp and MOPITT. Slope values are obtained using both data sets (red line).

GEOS-Chem model outputs are presented in Fig. 2 3 over the entire period from the beginning of 2009 until June 2013. The model is in good agreement with ground-based observations (reasonable correlation with R^2 between 0.53 and values of up to 0.69), even if the observed total atmospheric CO abundance is underestimated at all three sites: the relative deviations are commensurate: -24% for Paris, -21% for Jungfraujoch, and -20% for Wollongong. In Duncan et al. (2007), the averaged bias between observations and GEOS-Chem model simulations is less than $\pm 10\%$, but for some sites (Seychelles or Tae-Ahn), the bias can exceed $\pm 20\%$. Zeng et al. (2015) have observed large underestimations from models as compared to the ground-based FTIR stations in the Southern Hemisphere ranging from -19.2% to -27.5% and depending on the emission inventories

[3] https://lta.cr.usgs.gov/GTOPO30 (Global 30 Arc-Second Elevation)

implemented in the models for the Wollongong site (episodic events unaccounted for in the emission inventories). The present deviations are also ~~These deviations are~~ consistent with previous inverse modeling studies (Kopacz et al., 2010; Hooghiemstra et al., 2012) and could originate from an underestimation of the emissions of CO and of its VOC precursors in the inventories currently implemented in GEOS-Chem. Nonetheless, exploring this discrepancy was beyond the scope of this paper that aims at studying the seasonal variability of CO and not at reproducing observed concentrations. It has thus to be underlined that the model shows the same seasonal variability as the measurements: GEOS-Chem simulations reproduce the Northern Hemispheric maximum in March-April and the minimum in September-October and ~~. Therefore,~~ the model is therefore appropriate for diagnosing the seasonal variability. Both, the period and the relative amplitude of the variability are comparable to the measurement results, cf. Table 2. The lower R^2 ~~correlation factor~~ between GEOS-Chem and ground-based FTIR for Jungfraujoch and Wollongong as compared to Paris, are probably due to the more complex orography at these two sites: Jungfraujoch is located in the highest Swiss Alps and the surroundings show very large differences in altitude; Wollongong is sandwiched between the ocean (Tasman sea) and a hilly region (Blue mountains) with a typical altitude of a few hundred meters.

4.2 In situ measurements of surface CO

Daily averages of the surface CO concentration during the $2009-2013$ period at Paris are plotted in the bottom panel of Fig. 4. Since only very few FTS-Paris data are available for the winter months January and December, the corresponding monthly means have not been presented in Fig. 4~~5 (bottom panel) in dark green crosses~~.

~~Days with strong local influence, indicated by a VMR greater than 1ppmv, are excluded from the analysis.~~ The figure shows a clear seasonal variability with a maximum around January-February and a minimum around July-August. The amplitude of the seasonal variation is about 30%, which is larger ~~higher~~ than the total column variability. This shows the stronger and more direct influence of ~~the~~ local CO emissions due to ~~emission due to the~~ anthropogenic activities, which are expected to be particularly high in a megacity. As mentioned in Sect. 2.1, the retrieval grid (49 levels) provides a much thinner atmospheric layering than the effective vertical resolution indicated by the averaging kernels (Rodgers, 1990). The CO averaging kernels for each altitude of the a priori profile ~~averaging kernels~~ indicate a good sensitivity of the FTS-Paris instrument to the PBL. Effectively, the left panel of the figure 5 shows that the retrieval of CO essentially provides two independent measurement points of tropospheric CO: the first point supplies maximal information in the altitude range between 0 and 1000 m and thus well represents the PBL. The second one is representative of the upper troposphere, with a maximum around 8-9 km. The FTS-Paris data in the bottom panel of ~~The magenta stars in~~ Fig. 4 5 ~~(bottom panel)~~ represent the averaged CO VMR obtained ~~by the remote sensing measurements~~ for the altitude range between the ground (60 m asl~~height~~) and the 1000 m level. These ~~The~~ remote sensing measurements are consistent with the in situ data, even if they are

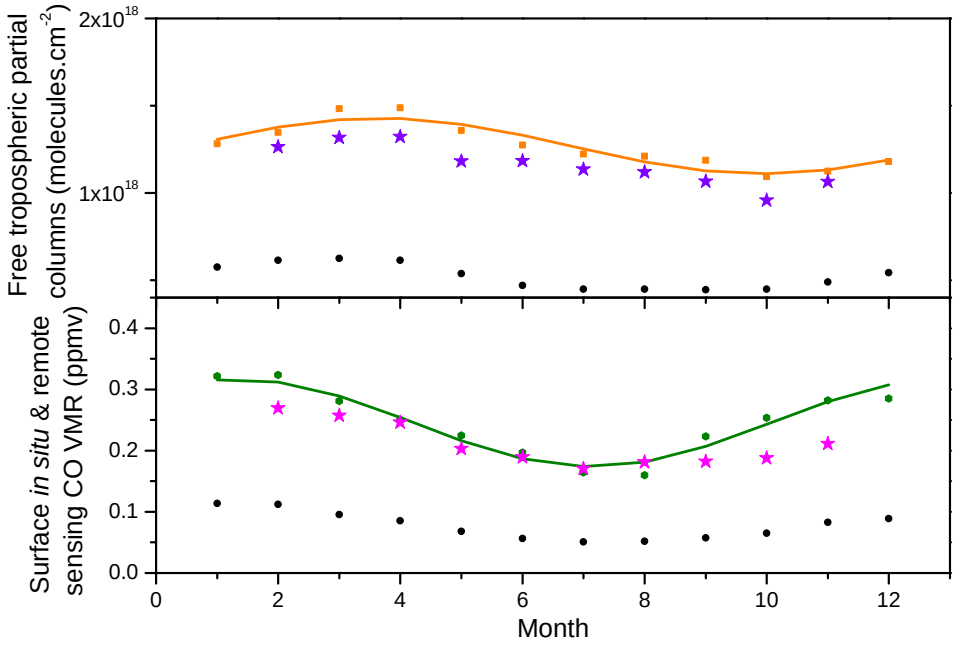

Figure 4. Free tropospheric (top) and surface (bottom) CO at Paris as monthly averages over 5 years. CO VMR in the PBL come from the in situ CO analyser (dark green hexagons) and from the FTS-Paris (magenta stars), as well as from the ~~Correlation between~~ GEOS-Chem model (black circles). Free tropospheric CO ~~and ground-based FTIR total~~ columns were calculated between 2 and 12 km and monthly averaged over ~~at~~ the period from 2009 to 2013. Shown are data from IASI-MetOp (orange squares), FTS-Paris (purple stars) and from GEOS-Chem modeling (black circles). A sine function fit is applied to the IASI-MetOp (orange line) and in situ CO data (dark green line)~~three different sites~~.

much less affected by local pollution peaks. By comparing Figs. 1 and 4~~2 and 5~~, we notice that the seasonal variability of the total column is shifted by about 2 months as compared to the variability at the surface. The ~~In order to study the~~ free tropospheric columns of CO have been calculated as partial columns ~~, we have recalculated the partial columns of~~ between 2 and about 12 km over Paris for both, ~~, obtained by the ground-based FTS-Paris and the satellite~~ IASI-MetOp and FTS-Paris. The right panel of the figure 5 shows the July 2010 monthly averaged AVKs of IASI-MetOp. These AVKs show a relatively low surface sensitivity which is more emphasised during winter (we have also checked the January 2010 monthly averaged AVKs not shown here).We thus only exploit the partial columns corresponding to the free troposphere~~instruments. Figure 5 (top panel)compares these free tropospheric partial columns with the output from GEOS-Chem~~. The seasonal variability in the free troposphere obtained by the three different kinds of data is also shifted by two months as compared to the surface seasonal variation. In addition to local surface sources, column abundances

are influenced by the transport of down wind emission sources~~As the average lifetime of is estimated to be about two to three months, the seasonal variation of the in the atmosphere is not only due to local emissions, but also due to other natural and anthropogenic contributions: biomass burning, long distance transport , chemical processes, i.e. oxidization of methane~~. The surface seasonal variability is directly influenced by the local emission due to human activities: fossil fuel combustion, domestic heating~~warming system~~, and industrial activities. In contrast, ~~comparison~~ the total column seasonal variability is additionally influenced by emissions from distant sources that get transported into ~~distant sources transported to~~ the upper levels of the atmosphere. ~~At Paris, the seasonality introduced by these distant sources outweighs the contribution of the local surface.~~ The surface CO maximum in January-February corresponds to the winter season, where domestic heating is strong and ~~,~~ where the PBL height is reduced. Additionally, ~~and when~~ oxidation by OH is lowest due to weak actinic flux. The minimum in July-August, where the PBL height is highest, not only corresponds to an increased oxidization of CO by OH, whose abundance is influenced by solar ultraviolet radiation (Bousquet et al., 2005; Rohrer and Berresheim, 2006; Duncan et al., 2007), but also to ~~corresponds to~~ the summer vacation season during which the inhabitants of Paris ~~Paris inhabitants~~ usually leave the city (by more than 50%, http://www.insee.fr), leading to a drastic decrease of vehicle traffic. In order to check the consistency of the GEOS-Chem model, we have plotted the GEOS-Chem surface VMR in the bottom panel of the Fig. 4~~5~~. The model confirms the time shift between surface and total column seasonal variability, with a maximum at the end of January-February and a minimum at the end of July-August. We once again notice an underestimation of the surface CO VMR by the GEOS-Chem model. The discrepancy of about -37% is larger than the difference of -24% between GEOS-Chem and ground-based total columns, and can probably be attributed to strong local emissions, which are not in the current emission inventories implemented in GEOS-Chem.

There is also a temporal shift in seasonal cycles between the surface and the ~~surface and~~ high altitudes in Switzerland, as indicated by the difference between urban and mountain sites. This is shown in Figure 6 that compares the four urban NABEL ~~NABEL urban~~ sites with an average altitude of 438.25 m asl to ~~with~~ the in situ surface CO obtained on top of Jungfraujoch at the ~~at Jungfraujoch with an~~ altitude of 3578 m asl. The low-altitude sites ~~low altitude sites located in urban areas~~ show a similar seasonal variability to ~~as~~ the surface CO at Paris, with a maximum around January and a minimum around July. Zellweger et al. (2009) point out that the in situ observations at Swiss urban stations reliably represent the mixture of traffic and industrial emissions.

Quite differently, in situ surface CO at Jungfraujoch shows ~~The surface seasonal variation is deeply impacted and driven by local anthropogenic emissions. In comparison, the high altitude NABEL site at Jungfraujoch presents~~ the same seasonal variability as ~~of~~ the whole atmosphere (characterized by ~~as observed in~~ the total column seasonality) being shifted by ~~with a time shift of~~ 2 months with respect to the urban sites. This is in agreement with the ~~. The~~ GEOS-Chem modeling ~~monthly averaged surface VMR shows similar variability as compared to the NABEL surface data~~ at

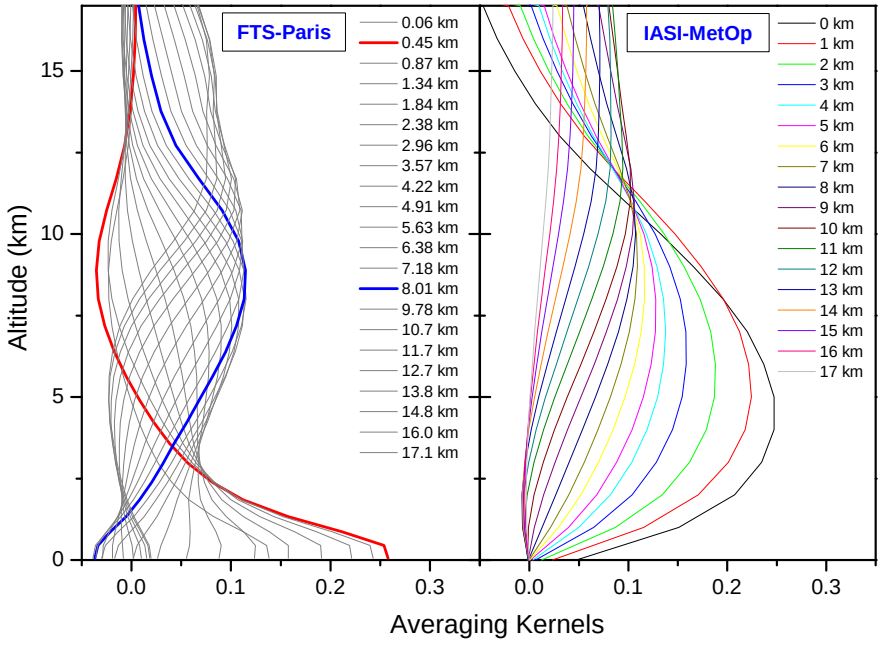

Figure 5. CO averaging kernels for each altitude of ~~VMR in~~ the a priori profile ~~PBL (bottom panel)~~ from 0 to 17 km~~surface in situ (dark green crosses)~~ for ~~and~~ FTS-Paris (left ~~magenta stars) data, and from GEOS-Chem model (black circles). Free tropospheric CO columns (top~~ panel) ~~were calculated between 2~~ and ~~12 km, from~~ IASI-MetOp (right panel~~orange squares) and FTS-Paris (purple stars) measurements as well as from GEOS-Chem (black circles)at Paris~~.

Jungfraujoch. Unlike the modeling for Paris where the underestimation is much stronger~~Paris case~~, the GEOS-Chem underestimates ~~underestimation for~~ the CO surface VMR by about 23~~is about −23~~%, which is similar to the 21~~difference of −21~~% difference obtained for the total columns. This is consistent with the much lower ~~, being consistent with much less~~ influence from low altitude emissions and from the PBL.

Figure 7 shows the monthly averaged surface CO in situ measurements performed at Wollongong between June 2012 and May 2013. We observe a surface seasonality with a maximum around October and a minimum in February-March. The maximum corresponds to elevated biomass burning levels during the Southern Hemispheric spring ~~summer~~ (Edwards et al., 2006). Unlike the two Northern Hemispheric sites, there seems to be ~~This is confirmed by the GEOS-Chem simulation performed without biomass burning emissions, in which the simulated seasonality at Wollongong is largely reduced (see Sect. 4.3). The after March increase during the end of autumn and at the beginning of the winter season corresponds to increased anthropogenic emissions (heating and traffic). The secondary minimum in July can possibly be explained by a reduced influence of local emissions~~

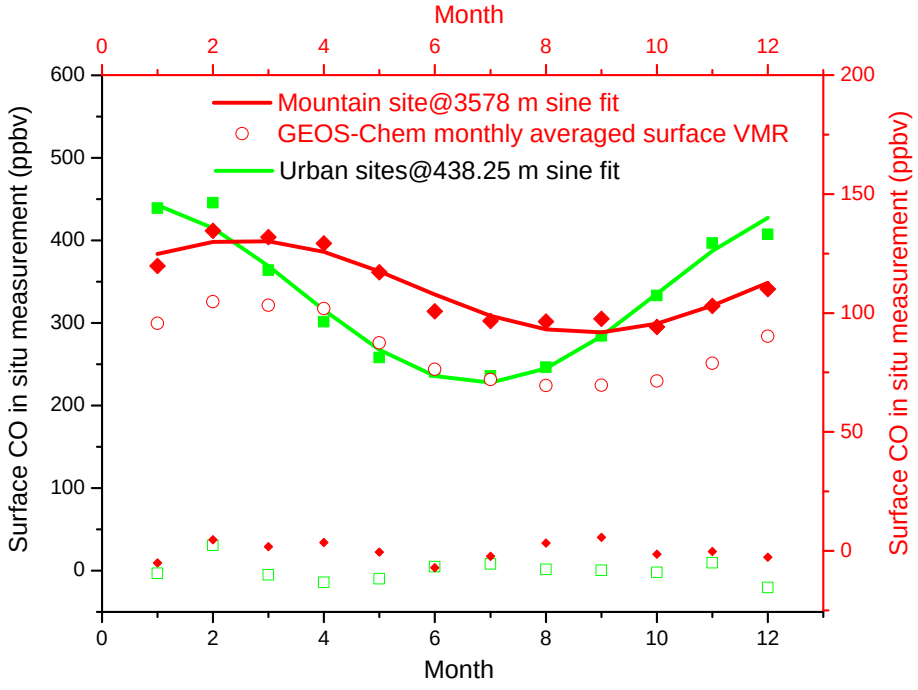

Figure 6. 5 years monthly averaged CO in situ measurements at the surface in Switzerland using Swiss NABEL data from 2009 to 2013 (green squares for the four urban sites means and red diamonds for Jungfraujoch). The sine function fit is applied on the 5 years monthly means of urban sites (green line) and of mountain site (red line). The below part shows the residuals of the fit (green open squares for urban sites and red small diamonds for Jungfraujoch). Monthly averaged CO surface VMR from GEOS-Chem model located at Jungfraujoch (red open circles).

~~from cars on the university campus (where the measurements are made) during the winter university vacation period. It seems that there is~~ no significant time shift between the CO seasonal variabilities at the Wollongong surface level and at higher altitudes. This suggests that the Wollongong surface atmosphere is more ~~generally~~ representative of the free troposphere. The GEOS-Chem monthly averaged surface VMR shows a maximum during the austral spring and a lower level after the end of the austral summer until the austral winter. A striking increase after March 2013 is observed by the surface in situ measurements, but not by the GEOS-Chem model. This might be due to close-by local emission sources which are probably not referenced in the inventories implemented in GEOS-Chem. A longer time series of these measurements will be helpful to better understand this observation. The background seasonality of CO is mainly driven by biomass burning sources modulated by the OH sink, (Buchholz et al., 2016). Similar to Paris, the surface CO discrepancy between model and measurement of -33% is slightly increased as compared to the value of -20% for the total columns.

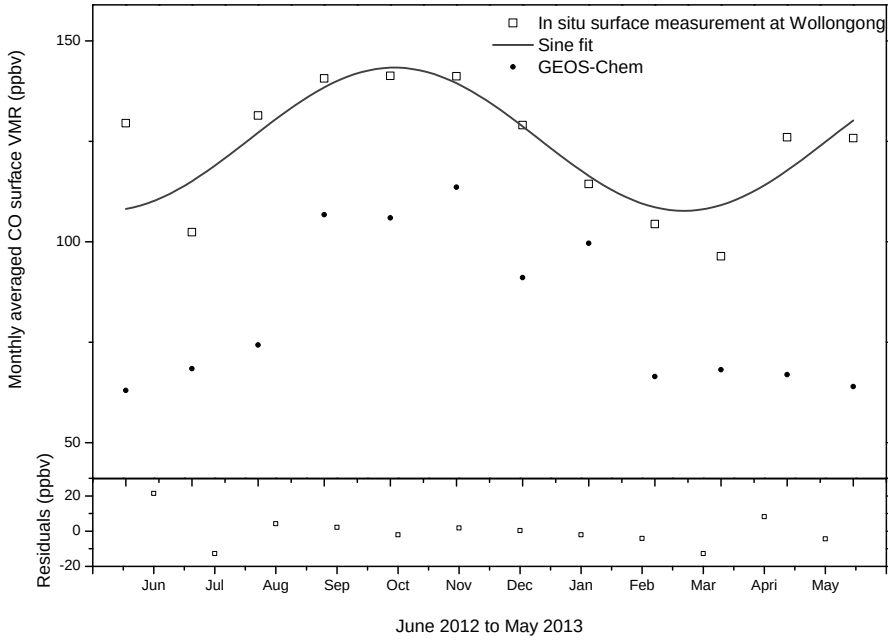

Figure 7. Monthly averaged CO surface VMR at Wollongong from in situ measurements (black open squares) and from GEOS-Chem model (black full circles) from June 2012 to May 2013. The sine function fit residuals are shown in the bottom panel.

4.3 Emission sources impacting the seasonality of CO columns

In order to study the influence of the different categories of CO and NMVOC emissions on the CO total column and its seasonality at the three sites, another three GEOS-Chem simulations have been run~~were performed~~. These relied on the same setup as for the standard run (standard chemistry, horizontal resolution, time period…), but in each of these runs we turned off either the biogenic, the anthropogenic (incorporating the biofuel emissions) or the biomass burning emission sources ~~that are~~ implemented in the model. These categories include direct emissions of CO (for both anthropogenic and biomass burning sources) and its NMVOC precursor emissions~~of its NMVOC precursors~~, as well as direct emissions of nitric oxide (NO). In these three sensitivity runs – hereafter referred to ~~, concentrations are provided by the NOAA measurements. Hereafter, they are referred to ,~~ as the non-biogenic, non-anthropogenic and non-biomass burning simulations – CH_4 concentrations are based on measurements from NOAA. The results of ~~from~~ these GEOS-Chem sensitivity simulations are compared to the standard run (results shown in Fig. 2~~3~~). All four runs cover the mid-2005 to mid-2013 time period, hence starting a few years before our ~~the~~ period under investigation~~here~~. This allows us to establish a stable situation for the period ~~after~~ 2008 (most of the long-lived precursors of

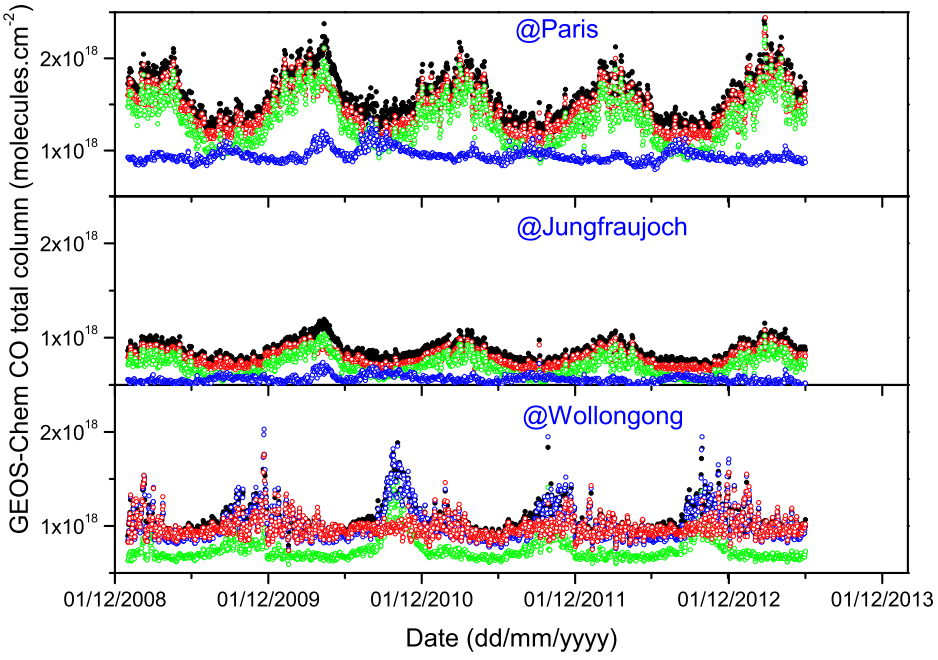

Figure 8. GEOS-Chem time series of CO total columns for Paris (top~~panel~~), Jungfraujoch (middle~~panel~~) and Wollongong (bottom~~panel~~). Different colors indicate standard run (black), run without biomass burning (red), run without biogenic emissions (green) and run without anthropogenic emissions (blue).

CO are removed from the atmosphere between mid-2005 and 2008). Figure~~Fig.~~ 8 shows the CO total columns simulated by the different runs of GEOS-Chem for the three sites. The ~~: the standard run in small black circles, together with the non-biomass burning, non-biogenic and non-anthropogenic runs in red, green and blue circles, respectively. According to the GEOS-Chem simulations, the~~ results for Paris and Jungfraujoch are quite similar. At these two sites, the seasonal variability of the CO loadings is mainly driven by anthropogenic emissions. Indeed, by shutting off the anthropogenic emissions of CO and of its NMVOC precursors, the amplitude of the CO seasonal variation and periodicity are radically reduced. This is in agreement with previous model studies. Duncan et al. (2007) show that fossil fuel emissions are the main contribution to the CO burden in the Northern extra-tropics. The high-altitude Jungfraujoch site is strongly impacted by long-range transport of CO. At least one third of it is of non-European origin (Duncan et al., 2007; Zellweger et al., 2009). Inversely, shutting off ~~On the other hand, without~~ either biomass burning or biogenic emissions, only weakly affect the seasonal cycle and the maximum peaks. As ~~maximum peaks are only weakly affected as~~ compared to the standard run, ~~with~~ CO columns are just a little bit ~~slightly~~ lower due to some emissions missing~~missing emissions~~. At Wollongong, the seasonal variability is mainly influenced by the biomass burning emissions: the highest peaks (e.g. at the end of 2009) disappear when

the biomass burning component is removed from the simulation. The biogenic emissions provide the largest ~~more of a large~~ background contribution. Zeng et al. (2015) have observed that the impact of biogenic emissions on CO is larger in the Southern Hemisphere than in the Northern. Unlike at Paris and Jungfraujoch, the influence of anthropogenic emissions is negligible in the Wollongong simulation. We also note that ~~anthropogenic emissions are negligible in Wollongong. For the surface VMR,~~ the GEOS-Chem sensitivity runs provide the same results for the CO surface VMR, as for ~~as compared to~~ the CO total columns at ~~for~~ the three studied sites.

5 Conclusions

This paper investigates the seasonal variability of CO total columns at three NDACC and/or TCCON sites: Paris and Jungfraujoch in the Northern Hemisphere and Wollongong in the Southern Hemisphere. In the Northern Hemisphere, the ~~The~~ variability of CO above the PBL has a seasonal maximum in March-April and a minimum in September-October. In the Southern Hemisphere, this ~~in the Northern Hemisphere. This~~ seasonal cycle is shifted by 6 months~~in the Southern Hemisphere. For both Northern-hemispheric sites, the seasonal variability of the total columns seems to be mainly driven by anthropogenic emissions. On the contrary, the Southern-hemispheric site Wollongong is mainly influenced by the biomass burning contribution~~. We have compared the ground-based FTIR data to satellite measurements from IASI-MetOp and MOPITT and to GEOS-Chem model standard outputs, which ~~all of them~~ confirm the observed CO seasonal variability. However with currently implemented inventories, an underestimation of about 20% by the ~~The~~ GEOS-Chem model is observed, which is consistent with previous forward and inverse modelling studies. Interestingly, a time-lag of about 2 months between upper altitude and surface CO has been found in both Paris and Jungfraujoch. This time lag is likely linked to the different emission patterns. Custom simulations with emission sources being individually turned on and off show ~~also shows~~ that the CO seasonality at Paris and Jungfraujoch is mainly controlled by anthropogenic emissions. In ~~This is different to~~ Wollongong, where low ~~it is due to biomass burning. For sites that are strongly affected by~~ local anthropogenic emissions prevail and where the impact of biomass burning and biogenic emissions is large, such a time shift is neither observed nor modelled. We have thus ~~, we have~~ observed a temporal shift in the seasonal patterns at the surface and in the higher atmospheric layers for the sites that are strongly affected by local anthropogenic emissions. The observation of the time-lag is likely due to zonal mixing occurring ~~. This is likely because zonal mixing occurs~~ on a shorter (1–2 weeks) timescale as ~~compared to~~ complete vertical tropospheric mixing (1–2 months). In the future, it will be interesting to study more closely the link between local and non-local emission sources and the magnitude of the time shift between surface and total column ~~The observed time-lag between upper altitude and surface~~ CO by extending the present study on more sites and to improve the analysis of the temporal signals. The presence of global ground-based FTIR networks provides a unique

opportunity to obtain these data on a global scale, as the instruments are capable of studying the surface and the total column data at the same time. The time lag data might also provide an additional benchmark parameter for chemical transport models and emission inventories, taking into account that the modeling of vertical CO gradients in the remote Southern Hemisphere already provides a challenge for chemical transport modeling (Fisher et al., 2015). ~~is about 2 months in Paris and at the Jungfraujoch. The 2 months' shift is also confirmed by the GEOS-Chem model. In Wollongong, where low local anthropogenic emissions prevail and which is largely impacted by biomass burning, such a time shift is neither observed nor modelled.~~

Acknowledgements. We are grateful to Université Pierre et Marie Curie and Région Île-de-France for their financial contributions and to Institut Pierre-Simon Laplace for support and facilities. We thank the National Center for Atmospheric Research MOPITT science team and NASA for producing and archiving the MOPITT CO product. Thanks are also due to the Swiss National Air Pollution Monitoring Network (NABEL) for delivering ground data around Switzerland. The University of Liège contribution to the present work has primarily been supported by the F.R.S. – FNRS, the Fédération Wallonie-Bruxelles and MeteoSwiss (GAW-CH program). We thank the International Foundation High Altitude Research Stations Jungfraujoch and Gornergrat (HFSJG, Bern). We are grateful to all colleagues who contributed to the acquisition of the FTIR data. The NDACC datasets used here are publicly available from the network database (ftp://ftp.cpc.ncep.noaa.gov/ndacc/station). The Australian Research Council has provided financial support over the years for the NDACC site at Wollongong, most recently as part of project DP110101948. We also acknowledge the important contribution to the measurement program at Wollongong made by researchers other than those listed as co-authors here, including amongst others, Voltaire Velazco and Nicholas Deutscher. IASI has been developed and built under the responsibility of the French space agency CNES. It is flown onboard the MetOp satellite as part of the Eumetsat Polar System (EPS). The IASI L1 data are received through the Eumetcast near real time data distribution service. IASI L1 and L2 data are stored in the French atmospheric database Ether (http://ether.ipsl.jussieu.fr). The National Center for Atmospheric Research (NCAR) is sponsored by the National Science Foundation. Any opinions, findings and conclusions or recommendations expressed in the publication are those of the author(s) and do not necessarily reflect the views of the National Science Foundation.

[Table 1 about here.]

[Table 2 about here.]

References

August, T., Klaes, D., Schlüssel, P., Hultberg, T., Crapeau, M., Arriaga, A., O'Carroll, A., Coppens, D., Munro, R., and Calbet, X.: IASI on MetOp-A: Operational Level 2 retrievals after five years in orbit, J. Quant. Spectroscop. Radiat. Transfer, 113, 1340–1371, doi:10.1016/j.jqsrt.2012.02.028, 2012.

Bakwin, P. S., Tans, P. P., and Novelli, P. C.: Carbon monoxide budget in the northern hemisphere, Geophs. Res. Lett., 21, 433—436, 1994.

Barret, B., Mazière, D. M., and Mahieu, E.: Ground-based FTIR measurements of CO from the Jungfraujoch: characterisation and comparison with in situ surface and MOPITT data, Atmos. Chem. Phys., 3, 2217–2223, doi:10.5194/acp-3-2217-2003, 2003.

Bekki, S., Law, K. S., and Pyle, J. A.: Effect of ozone depletion on atmospheric CH_4 and CO concentrations, Nature, 371, 595–597, doi:10.1038/371595a0, 1994.

Benedictow, A., Berge, H., Fagerli, H., Gauss, M., Jonson, J. E., Nyíri, A., Simpson, D., Tsyro, S., Valdebenito, A., Shamsudheen, V. S., Wind, P., Aas, W., Hjellbrekke, A.-G., Mareckova, K., Wankmüller, R., Iversen, T., Kirkevøag, A., Seland, Ø., Haugen, J. E., and Mills, G.: Transboundary acidification, eutrophication and ground level ozone in Europe in 2008, Tech. rep., The Norwegian Meteorological Institute, Oslo, Norway, 2010.

Bey, I., Jacob, D. J., Yantosca, R. M., Logan, J. A., Field, B. D., Fiore, A. M., Li, Q., Liu, H. Y., Mickley, L. J., and Schultz, M. G.: Global modeling of tropospheric chemistry with assimilated meteorology: model description and evaluation, J. Geophys. Res.-Atmos., 106, 23 073–23 095, doi:10.1029/2001JD000807, 2001.

Blumstein, D., Chalon, G., Carlier, T., Buil, C., Hebert, P., Maciaszek, T., Ponce, G., Phulpin, T., Tournier, B., Simeoni, D., Astruc, P., Clauss, A., Kayal, G., and Jegou, R.: IASI instrument: technical overview and measured performances, in: Proc. SPIE 5543, Infrared Spaceborne Remote Sensing XII, doi:10.1117/12.560907, 2004.

Bousquet, P., Hauglustaine, D. A., Peylin, P., Carouge, C., and Ciais, P.: Two decades of OH variability as inferred by an inversion of atmospheric transport and chemistry of methyl chloroform, Atmos. Chem. Phys., 5, 2635–2656, doi:10.5194/acp-5-2635-2005, 2005.

Brunke, E.-G., Scheel, H., and Seiler, W.: Trends of tropospheric CO, N_2O and CH_4 as observed at cape point, South Africa, Atmos. Environ., 24, 585–595, doi:10.1016/0960-1686(90)90013-D, 1990.

Buchholz, R. R., Paton-Walsh, C., Griffith, D. W. T., Kubistin, D., Caldow, C., Fisher, J. A., Deutscher, N. M., Kettlewell, G., Riggenbach, M., Macatangay, R., Krummel, P. B., and Langenfelds, R. L.: Source and meteorological influences on air quality (CO, CH_4 & CO_2) at a Southern Hemisphere urban site, Atmos. Environ., 126, 274–289, doi:10.1016/j.atmosenv.2015.11.041, 2016.

Clerbaux, C., George, M., Turquety, S., Walker, K. A., Barret, B., Bernath, P., Boone, C., Borsdorff, T., Cammas, J. P., Catoire, V., Coffey, M., Coheur, P.-F., Deeter, M., Mazière, D. M., Drummond, J., Duchatelet, P., Dupuy, E., Zafra, d. R., Eddounia, F., Edwards, D. P., Emmons, L., Funke, B., Gille, J., Griffith, D. W. T., Hannigan, J., Hase, F., Höpfner, M., Jones, N., Kagawa, A., Kasai, Y., Kramer, I., Flochmoën, L. E., Livesey, N. J., López-Puertas, M., Luo, M., Mahieu, E., Murtagh, D., Nédélec, P., Pazmino, A., Pumphrey, H., Ricaud, P., Rinsland, C. P., Robert, C., Schneider, M., Senten, C., Stiller, G., Strandberg, A., Strong, K., Sussmann, R., Thouret, V., Urban, J., and Wiacek, A.: CO measurements from the ACE-FTS satellite instrument: data

analysis and validation using ground-based, airborne and spaceborne observations, Atmos. Chem. Phys., 8, 2569–2594, doi:10.5194/acp-8-2569-2008, 2008.

Clerbaux, C., Boynard, A., Clarisse, L., George, M., Hadji-Lazaro, J., Herbin, H., Hurtmans, D., Pommier, M., Razavi, A., Turquety, S., Wespes, C., and Coheur, P.-F.: Monitoring of atmospheric composition using the thermal infrared IASI/MetOp sounder, Atmos. Chem. Phys., 9, 6041–6054, doi:10.5194/acp-9-6041-2009, 2009.

Deeter, M., Emmons, L., Francis, G., Edwards, D., Gille, J., Warner, J., Khattatov, B., Ziskin, D., Lamarque, J.-F., Ho, S.-P., Yudin, V., Attié, J.-L., Packman, D., Chen, J., Mao, D., Drummond, J., Novelli, P., and Sachse, G.: Evaluation of operational radiances for the Measurements of Pollution in the Troposphere (MOPITT) instrument CO thermal band channels, J. Geophys. Res., 109, D03 308, doi:10.1029/2003JD003970, 2004.

Dils, B., Cui, J., Henne, S., Mahieu, E., Steinbacher, M., and Mazière, D. M.: CO trend at the high Alpine site Jungfraujoch: a comparison between NDIR surface in situ and FTIR remote sensing observations, Atmos. Chem. Phys., 11, 6735–6748, doi:10.5194/acp-11-6735-2011, 2011.

Drummond, J. and Mand, G.: The Measurements of Pollution in the Troposphere (MOPITT) Instrument: Overall Performance and Calibration Requirements, J. Atmos. Ocean. Technol., 13, 314, 1996.

Duchatelet, P., Demoulin, P., Hase, F., Ruhnke, R., Feng, W., Chipperfield, M. P., Bernath, P. F., Boone, C. D., Walker, K. A., and Mahieu, E.: Hydrogen fluoride (HF) total and partial column time series above the Jungfraujoch from long-term FTIR measurements: impact of the line-shape model, error budget, seasonal cycle and comparison with satellite and model data, J. Geophys. Res., 115, D22 306, doi:10.1029/2010JD014677, 2010.

Duncan, B. N., Logan, J. A., Bey, I., Megretskaia, I. A., Yantosca, R. M., Novelli, P. C. Jones, N. B., and Rinsland, C. P.: Global budget of CO, 1988–1997: Source estimates and validation with a global model, J. Geophys. Res. Atmos., 112, doi:10.1029/2007JD008459, d22301, 2007.

Edwards, D. P., Pétron, G., Novelli, P. C., Emmons, L. K., Gille, J. C., and Drummond, J. R.: Southern Hemisphere carbon monoxide interannual variability observed by Terra/Measurement of Pollution in the Troposphere (MOPITT), J. Geophys. Res., 111, D16 303, doi:10.1029/2006JD007079, 2006.

Esposito, F., Grieco, G., Masiello, G., Pavese, G., Restieri, R., Serio, C., and Cuomo, V.: Intercomparison of line-parameter spectroscopic databases using downwelling spectral radiance, Quart. J. Roy. Met. Soc., 133, 191–202, doi:10.1002/qj.131, 2007.

Fisher, J. A., Wilson, S. R., Zeng, G., Williams, J. E., Emmons, L. K., Langenfelds, R. L., Krummel, P. B., and Steele, L. P.: Seasonal changes in the tropospheric carbon monoxide profile over the remote Southern Hemisphere evaluated using multi-model simulations and aircraft observations, Atmos. Chem. Phys., 15, 3217–3239, doi:10.5194/acp-15-3217-2015, 2015.

George, M., Clerbaux, C., Hurtmans, D., Turquety, S., Coheur, P.-F., Pommier, M., Hadji-Lazaro, J., Edwards, D. P., Worden, H., Luo, M., Rinsland, C., and McMillan, W.: Carbon monoxide distributions from the IASI/METOP mission: evaluation with other space-borne remote sensors, Atmos. Chem. Phys., 9, 8317–8330, doi:10.5194/acp-9-8317-2009, 2009.

Griffith, D. W. T.: Synthetic Calibration and Quantitative Analysis of Gas-Phase infrared Spectra, Appl. Spectroscop., 50, 59–70, 1996.

Griffith, D. W. T., Deutscher, N. M., Caldow, C. G. R., Kettlewell, G., Riggenbach, M., and Hammer, S.: A Fourier transform infrared trace gas and isotope analyser for atmospheric applications, Atmos. Meas. Tech., 5, 2012.

Guenther, A., Karl, T., Harley, P., Wiedinmyer, C., Palmer, P. I., and Geron, C.: Estimates of global terrestrial isoprene emissions using MEGAN (Model of Emissions of Gases and Aerosols from Nature), Atmos. Chem. Phys., 6, 10–5194, 2006.

Hase, F., Hannigan, J. W., Coey, M. T., Goldman, A., Höpfner, M., Jones, N. B., Rinsland, C. P., and Wood, S. W.: Intercomparison of retrieval codes used for the analysis of high-resolution: ground-based FTIR measurements, J. Quant. Spectroscop. Radiat. Transfer, 87, 25–52, 2004.

Hase, F., Demoulin, P., Sauval, A. J., Toon, G. C., Bernath, P. F., Goldman, A., Hannigan, J. W., and Rinsland, C. P.: An empirical line-by-line model for the infrared solar transmittance spectrum from 700 to 5000 cm^{-1}, J. Quant. Spectroscop. Radiat. Transfer, 102, 450–463, doi:10.1016/j.jqsrt.2006.02.026, 2006.

Holloway, T., Levy, H., and Kasibhatla, P.: Global distribution of carbon monoxide, J. Geophys. Res. Atmos., 105, 12 123–12 147, doi:10.1029/1999JD901173, 2000.

Hooghiemstra, P. B., Krol, M. C., Bergamaschi, P., de Laat, A. T. J., van der Werf, G. R., Novelli, P. C., Deeter, M. N., Aben, I., and Röckmann, T.: Comparing optimized CO emission estimates using MOPITT or NOAA surface network observations, J Geophys. Res., 117, D06 309–23, 2012.

Hurtmans, D., Coheur, P.-F., Wespes, C., Clarisse, L., Scharf, O., Clerbaux, C., Hadji-Lazaro, J., George, M., and Turquety, S.: FORLI radiative transfer and retrieval code for IASI, J. Quant. Spectroscop. Radiat. Transfer, 113, 1391–1408, doi:10.1016/j.jqsrt.2012.02.036, 2006.

Khalil, M. A. K. and Rasmussen, R. A.: Carbon monoxide in the Earth's atmosphere: indications of a global increase, Nature, 332, 242–245, doi:10.1038/332242a0, 1988.

Khalil, M. A. K. and Rasmussen, R. A.: Global decrease in atmospheric carbon monoxide concentration, Nature, 370, 639–641, doi:10.1038/370639a0, 1994.

Kopacz, M., Jacob, D. J., Fisher, J. A., Logan, J. A., Zhang, L., Megretskaia, I. A., Yantosca, R. M., Singh, K., Henze, D. K., Burrows, J. P., Buchwitz, M., Khlystova, I., McMillan, W. W., Gille, J. C., Edwards, D. P., Eldering, A., Thouret, V., and Nedelec, P.: Global estimates of CO sources with high resolution by adjoint inversion of multiple satellite datasets (MOPITT, AIRS, SCIAMACHY, TES), Atmos. Chem. Phys., 10, 855–876, 2010.

Logan, J. A., Prather, M. J., Wofsy, F. C., and McElroy, M. B.: Tropospheric Chemistry: A Global Perspective, J. Geophys. Res., 86, 7210–7254, 1981.

Mahieu, E., Zander, R., Delbouille, L., Demoulin, P., Roland, G., and Servais, C.: Observed Trends in Total Vertical Column Abundances of Atmospheric Gases from IR Solar Spectra Recorded at the Jungfraujoch, J. Atmos. Chem., 28, 227–243, doi:10.1023/A:1005854926740, 1997.

Mao, J., Jacob, D. J., Evans, M. J., Olson, J. R., Ren, X., Brune, W. H., Clair, S. J. M., Crounse, J. D., Spencer, K. M., Beaver, M. R., Wennberg, P. O., Cubison, M. J., Jimenez, J. L., Fried, A., Weibring, P., Walega, J. G., Hall, S. R., Weinheimer, A. J., Cohen, R. C., Chen, G., Crawford, J. H., McNaughton, C., Clarke, A. D., Jaeglé, L., Fisher, J. A., Yantosca, R. M., Sager, L. P., and Carouge, C.: Chemistry of hydrogen oxide radicals (HOx) in the Arctic troposphere in spring, Atmos. Chem. Phys., 10, 5823–5838, doi:10.5194/acp-10-5823-2010, 2010.

Novelli, P. C., Masarie, K. A., Tans, P. P., and Lang, P. M.: Recent Changes in Atmospheric Carbon Monoxide, Science, 263, 1587–1590, doi:10.1126/science.263.5153.1587, 1994.

Novelli, P. C., Masarie, K. A., and Lang, P. M.: Distributions and recent changes of carbon monoxide in the lower troposphere, J. Geophys. Res. Atmos., 103, 19 015–19 033, doi:10.1029/98JD01366, 1998.

Novelli, P. C., Masarie, K. A., Lang, P. M., Hall, B. D., Myers, R. C., and Elkins, J. W.: Reanalysis of tropospheric CO trends: Effects of the 1997–1998 wildfires, J. Geophys. Res. Atmos., 108, doi:10.1029/2002JD003031, 4464, 2003.

Olivier, J. G. J. and Berdowski, J. J. M.: Global emissions sources and sinks., in: The Climate System, edited by Berdowski, J., Guicherit, R., and Heij, B., pp. 33–78, A.A. Balkema Publishers/Swets & Zeitlinger Publishers, Lisse, The Netherlands, 2001.

Park, R. J., Jacob, D. J., Field, B. D., Yantosca, R. M., and Chin, M.: Natural and transboundary pollution influences on sulfate-nitrate-ammonium aerosols in the United States: implications for policy, J. Geophys. Res., 109, D15 204, doi:10.1029/2003JD004473, 2004.

Pougatchev, N. S. and Rinsland, C. P.: Spectroscopic study of the seasonal variation of carbon monoxide vertical distribution above Kitt Peak, J. Geophys. Res, 100, 1409–1416, 1995.

Rinsland, C. P., Jones, N. B., Connor, B. J., Logan, J. A., Pougatchev, N. S., Goldman, A., Murcray, F. J., Stephen, T. M., Pine, A. S., Zander, R., Mahieu, E., and Demoulin, P.: Northern and southern hemisphere ground-based infrared spectroscopic measurements of tropospheric carbon monoxide and ethane, J. Geophys. Res., 103, 28 197, doi:10.1029/98JD02515, 1998.

Rinsland, C. P., Goldman, A., Murcray, F. J., Stephen, T. M., Pougatchev, N. S., Fishman, J., David, S. J., Blatherwick, R. D., Novelli, P. C., Jones, N. B., and Connor, B. J.: Infrared solar spectroscopic measurements of free tropospheric CO, C_2H_6, and HCN above Mauna Loa, Hawaii: Seasonal variations and evidence for enhanced emissions from the Southeast Asian tropical fires of 1997–1998, J. Geophys. Res. Atmos., 104, 18 667–18 680, doi:10.1029/1999JD900366, 1999.

Rinsland, C. P., Mahieu, E., Zander, R., Demoulin, P., Forrer, J., and Buchmann, B.: Free tropospheric CO, C_2H_6, and HCN above central Europe: Recent measurements from the Jungfraujoch station including the detection of elevated columns during 1998, J. Geophys. Res., 105, 24 235–24 249, 2000.

Rinsland, C. P., Meier, A., Griffith, D. W. T., and Chiou, L. S.: Ground-based measurements of tropospheric CO, C2H6, and HCN from Australia at 34 °S latitude during 1997–1998, J. Geophys. Res. Atmos., 106, 20 913–20 924, doi:10.1029/2000JD000318, 2001.

Rinsland, C. P., Goldman, A., Hanniganc, J. W., Wood, S. W., Chiou, L. S., and Mahieu, E.: Long-term trends of tropospheric carbon monoxide and hydrogen cyanide from analysis of high resolution infrared solar spectra, J. Quant. Spectroscop. Radiat. Transfer, 104, 40–51, 2007.

Rodgers, C. D.: Characterization and error analysis of profiles retrieved from remote sounding measurements, J. Geophys. Res., 95, doi:10.1029/JD095iD05p05587, 1990.

Rodgers, C. D. and Connor, B. J.: Intercomparison of remote sounding instruments, J. Geophys. Res., 108, 4116–4129, doi:10.1029/2002JD002299, 2003.

Rohrer, F. and Berresheim, H.: Strong correlation between levels of tropospheric hydroxyl radicals and solar ultraviolet radiation, Nature, 442, 184–187, doi:10.1038/nature04924, 2006.

Rothman, L. S., Jacquemart, D., Barbe, A., Benner, D. C., Birk, M., Brown, L. R., Carleer, M. R., Chackerian, Jr, C., Chance, K., Coudert, L. H., Dana, V., Devi, V. M., Flaud, J.-M., Gamache, R. R., Goldman, A., Hartmann, J.-M., Jucks, K. W., Maki, A. G., Mandin, J.-Y., Massie, S. T., Orphal, J., Perrin, A., Rinsland, C. P., Smith, M. A. H., Tennyson, J., Tolchenov, R. N., Toth, R. A., Vander Auwera, J., Varanasi, P., and Wagner, G.: The HITRAN 2004 Molecular Spectroscopic Database, J. Quant. Spectrosc. Radiat. Trans., 96, 139 – 204, 2005.

Rothman, L. S., Gordon, I. E., Barbe, A., Benner, D. C., Bernath, P. F., Birk, M., Boudon, V., Brown, L. R., Campargue, A., Champion, J. P., Chance, K., Coudert, L. H., Dana, V., Devi, V. M., Fally, S., Flaud, J. M., Gamache, R. R., Goldman, A., Jacquemart, D., Kleiner, I., Lacome, N., Lafferty, W. J., Mandin, J. Y., Massie, S. T., Mikhailenko, S. N., Miller, C. E., Moazzen-Ahmadi, N., Naumenko, O. V., Nikitin, A. V., Orphal, J., Perevalov, V. I., Perrin, A., Predoi-Cross, A., Rinsland, C. P., Rotger, M., Simecková, M., Smith, M. A. H., Sung, K., Tashkun, S. A., Tennyson, J., Toth, R. A., Vandaele, A. C., and Vander Auwera, J.: The HITRAN 2008 molecular spectroscopic database, J. Quant. Spectrosc. Radiat. Trans., 110, 533–572, 2009.

Schneider, M., Yoshimura, K., Hase, F., and Blumenstock, T.: The ground-based FTIR network's potential for investigating the atmospheric water cycle, Atmos. Chem. Phys., 10, 3427–3442, 2010.

Schultz, M., Backman, L., Balkanski, Y., Bjoerndalsaeter, S., Brand, R., Burrows, J., Dalsoeren, S., de Vasconcelos, M., Grodtmann, B., Hauglustaine, D., Heil, A., Hoelzemann, J., Isaksen, I., Kaurola, J., Knorr, W., Ladstaetter-Weißenmayer, A., Mota, B., Oom, D., Pacyna, J., Panasiuk, D., Pereira, J., Pulles, T., Pyle, J., Rast, S., Richter, A., Savage, N., Schnadt, C., Schulz, M., Spessa, A., Staehelin, J., Sundet, J., Szopa, S., Thonicke, K., van het Bolscher, M., van Noije, T., van Velthoven, P., Vik, A., and Wittrock, F.: REanalysis of the TROpospheric chemical composition over the past 40 years – A long-term global modeling study of tropospheric chemistry, final report 48/2007, Max Planck Institute for Meteorology, Hamburg, Germany, 2007.

Street, J. O., Carroll, R. J., and Ruppert, D.: A Note on Computing Robust Regression Estimates via Iteratively Reweighted Least Squares, Am. Stat., 42, 152–154, doi:10.1080/00031305.1988.10475548, 1988.

Té, Y., Jeseck, P., Payan, S., Pépin, I., and Camy-Peyret, C.: The Fourier transform spectrometer of the UPMC University QualAir platform, Rev. Sci. Instrum., 81, 103 102–10, doi:10.1063/1.3488357, 2010.

Té, Y., Dieudonné, E., Jeseck, P., Hase, F., Hadji-Lazaro, J., Clerbaux, C., Ravetta, F., Payan, S., Pépin, I., Hurtmans, D., Pelon, J., and Camy-Peyret, C.: Carbon monoxide urban emission monitoring: a ground-based FTIR case study, J. Atmos. Oceanic Technol., 29, 911–921, doi:10.1175/JTECH-D-11-00040.1, 2012.

Thompson, A. M.: The oxidizing capacity of the earth's atmosphere: Probable past and future changes, Science, 286, 1157–1165, doi:10.1126/science.256.5060.1157, 1992.

Thompson, A. M., Huntley, M. A., and Stewart, R. W.: Perturbations to tropospheric oxidants, 1985–2035: 1. Calculations of ozone and OH in chemically coherent regions, J. Geophys. Res, 95, 9829–9844, doi:10.1029/JD095iD07p09829, 1990.

Tournier, B., Blumstein, D., Cayla, F.-R., and Chalon, G.: IASI level 0 and 1 processing algorithms description, in: Proc. 12th Int. TOVS Study Conf. (ITSC-XII), Lorne, VIC, Australia, 2002.

van der Werf, G. R., Randerson, J. T., Giglio, L., Collatz, G. J., Mu, M., Kasibhatla, P. S., Morton, D. C., DeFries, R. S., Jin, Y., and Leeuwen, v. T. T.: Global fire emissions and the contribution of deforestation,

savanna, forest, agricultural, and peat fires, Atmos. Chem. Phys., 10, 11 707–11 735, doi:10.5194/acp-10-11707-2010, 2010.

van Donkelaar, A., Martin, R. V., Leaitch, W. R., MacDonald, A. M., Walker, T. W., Streets, D. G., Zhang, Q., Dunlea, E. J., Jimenez, J. L., Dibb, J. E., Huey, L. G., Weber, R., and Andreae, M. O.: Analysis of aircraft and satellite measurements from the Intercontinental Chemical Transport Experiment (INTEX-B) to quantify long-range transport of East Asian sulfur to Canada, Atmos. Chem. Phys., 8, 10–5194, doi:10.5194/acp-8-2999-2008, 2008.

Viatte, C., Schneider, M., Redondas, A., Hase, F., Eremenko, M., Chelin, P., Flaud, J.-M., Blumenstock, T., and Orphal, J.: Comparison of ground-based FTIR and Brewer O_3 total column with data from two different IASI algorithms and from OMI and GOME-2 satellite instruments, Atmos. Meas. Tech., 4, 535–546, doi:10.5194/amt-4-535-2011, 2011.

Weinstock, B.: Carbon Monoxide: Residence Time in the Atmosphere, Science, 166, 224–225, 1969.

Worden, H. M., Deeter, M. N., Edwards, D. P., Gille, J. C., Drummond, J. R., and Nédélec, P.: Observations of near-surface carbon monoxide from space using MOPITT multispectral retrievals, J. Geophys. Res. Atmos., 115, doi:10.1029/2010JD014242, d18314, 2010.

Xiao, Y., Logan, J. A., Jacob, D. J., Hudman, R. C., Yantosca, R., and Blake, D. R.: Global budget of ethane and regional constraints on U.S. sources, J. Geophys. Res., 113, 21 306–10, doi:10.1029/2007JD009415, 2008.

Yurganov, L. N., Blumenstock, T., Grechko, E. I., Hase, F., Hyer, E. J., Kasischke, E. S., Koike, M., Kondo, Y., Kramer, I., Leung, F.-Y., Mahieu, E., Mellqvist, J., Notholt, J., Novelli, P. C., Rinsland, C. P., Scheel, H. E., Schulz, A., Strandberg, A., Sussmann, R., Tanimoto, H., Velazco, V., Zander, R., and Zhao, Y.: A quantitative assessment of the 1998 carbon monoxide emission anomaly in the Northern Hemisphere based on total column and surface concentration measurements, J. Geophys. Res. Atmos., 109, doi:10.1029/2004JD004559, d15305, 2004.

Yurganov, L. N., Duchatelet, P., Dzhola, A. V., Edwards, D. P., Hase, F., Kramer, I., Mahieu, E., Mellqvist, J., Notholt, J., Novelli, P. C., Rockmann, A., Scheel, H. E., Schneider, M., Schulz, A., Strandberg, A., Sussmann, R., Tanimoto, H., Velazco, V., Drummond, J. R., and Gille, J. C.: Increased Northern Hemispheric carbon monoxide burden in the troposphere in 2002 and 2003 detected from the ground and from space, Atmos. Chem. and Phys., 5, 563–573, doi:10.5194/acp-5-563-2005, 2005.

Zander, R., Demoulin, P., Ehhalt, D. H., Schmidt, U., and Rinsland, C. P.: Secular increase of the total vertical column abundance of carbon monoxide above central Europe since 1950, J. Geophys. Res. Atmos., 94, 11 021–11 028, doi:10.1029/JD094iD08p11021, 1989.

Zander, R., Mahieu, E., Demoulin, P., Duchatelet, P., Roland, G., Servais, C., Mazière, D. M., Reimann, S., and Rinsland, C. P.: Our changing atmosphere: Evidence based on long-term infrared solar observations at the Jungfraujoch since 1950, Sci. Tot. Environ., 391, 184–195, doi:10.1016/j.scitotenv.2007.10.018, 2008.

Zbinden, R. M., Thouret, V., Ricaud, P., Carminati, F., Cammas, J.-P., and Nédélec, P.: Climatology of pure tropospheric profiles and column contents of ozone and carbon monoxide using MOZAIC, Atmos. Chem. Phys., 13, 12 363–12 388, doi:10.5194/acp-13-12363-2013, 2013.

Zellweger, C., Hüglin, C., Klausen, J., Steinbacher, M., Vollmer, M., and Buchmann, B.: Inter-comparison of four different carbon monoxide measurement techniques and evaluation of the long-term carbon monoxide time series of Jungfraujoch, Atmos. Chem. Phys., 9, 3491–3503, doi:10.5194/acp-9-3491-2009, 2009.

Zeng, G., Williams, J. E., Fisher, J. A., Emmons, L. K., Jones, N. B., Morgenstern, O., Robinson, J., Smale, D., Paton-Walsh, C., and Griffith, D. W. T.: Multi-model simulation of CO and HCHO in the Southern Hemisphere: comparison with observations and impact of biogenic emissions, Atmos. Chem. Phys., 15, 7217–7245, 2015.

Zhao, Y., Kondo, Y., Murcray, F. J., Liu, X., Koike, M., Kita, K., Nakajima, H., Murata, I., and Suzuki, K.: Carbon monoxide column abundances and tropospheric concentrations retrieved from high resolution ground-based infrared solar spectra at 43.5°N over Japan, J. Geophys. Res., 102, 23 403–23 411, 1997.

Zhao, Y., Strong, K., Kondo, Y., Koike, M., Matsumi, Y., Irie, Y., Rinsland, H., C, P., Jones, N. B., Suzuki, K., Nakajima, H., Nakane, H., and Murata, I.: Spectroscopic measurements of tropospheric CO, C_2H_6, C_2H_2 and HCN in Northern Japan, J. Geophy. Res., 107, 4343, doi:10.1029/2001JD000748, 2002.

Table 1. Ground-based FTIR instrumental information and details concerning the configuration used to record the measurements at the three studied sites

	Paris	Jungfraujoch	Wollongong
Sun-tracker model	A547 (Bruker Optics)	Home made	A547 (Bruker Optics)
Sun-tracker accuracy	< 1 arcmin	< 6 arcmin	< 1 arcmin
Spectrometer	IFS 125HR	IFS 120HR	IFS 125HR
Network	TCCON with NDACC measurements	NDACC	NDACC and TCCON
Optical Path Difference	257 cm	114 to 175 cm	257 cm
Integration time	205 s (2 co-additions)	135 to 1035 s (depending on co-addition and OPD)	206 s (2 co-additions)
Entrance window	CaF_2 (instrument under vacuum)	None (instrument not under vacuum)	KBr (instrument under vacuum)
Beamsplitter	CaF_2	KBr	CaF_2
Optical filter	Yes	Yes	Yes
Detector	InSb	InSb	InSb
Spectral range	3.8 to 5.1 μm	4.4 to 6 μm	4.4 to 5.1 μm

Table 2. Parameters obtained from the sinusoidal fit of the seasonal variability to the CO total columns from ground-based, satellite and GEOS-Chem modeling data

	Paris		Jungfraujoch		Wollongong	
	Half-period (w) (days)	Amplitude (A) (%)	Half-period (w) (days)	Amplitude (A) (%)	Half-period (w) (days)	Amplitude (A) (%)
Ground-based	191 ± 3	14 ± 1	185 ± 1	12 ± 1	178 ± 1	17 ± 1
Satellite data	183 ± 1	14 ± 1	190 ± 2	12 ± 1	182 ± 1	16 ± 1
GEOS-Chem	183 ± 1	19 ± 1	182 ± 1	12 ± 1	180 ± 1	13 ± 1